First-principles calculations of defects in oxygen-deficient silica exposed to hydrogen

Peter E. Blöchl
IBM Research, Zurich Research Laboratory, CH-8803 Rüschlikon, Switzerland
(Received 14 January 2000)

Hydrogen-related defects and oxygen vacancies in silica are analyzed using first-principles density-functional calculations. Energetics, structures, charge-state levels, and hyperfine parameters are determined. These calculations identify the hydrogen bridge related to the E_4' center as the defect responsible for the stress-induced leakage current, a forerunner of dielectric breakdown of gate oxides in transistors.

I. INTRODUCTION

A major concern in silicon technology is the reliability of CMOS (complementary metal-oxide semiconductor) devices as they are scaled to smaller dimensions. Among the main problems is the stress-induced leakage current (SILC) through the oxide, which is considered a forerunner of dielectric breakdown. Dielectric breakdown determines the lifetime of logical devices. Recent extrapolations[1] indicate that, in order to fulfill the lifetime requirements, the gate oxide thickness will be limited to 2.2–2.6 nm, which interferes with the road map of the Semiconductor Industry Association for the scaling of MOSFET's (metal-oxide semiconductor field-effect transistors) within the next five years. Understanding the microscopic origin of the detrimental effects in gate oxides gives rise to the hope that guided modifications in the process may yield devices that can reliably be extended to smaller structures.

Degradation of MOS structures has been attributed to hydrogen diffusing to the oxide-semiconductor interface.[2,3] In this model, hydrogen is released from the metal-oxide interface by hot electrons and diffuses to the oxide-semiconductor interface, where it depassivates hydrogenated P_b centers, i.e., silicon-dangling-bond defects, right at the semiconductor oxide interface. In addition, low-field leakage currents are generated by exposure to atomic hydrogen.[4,5] These still uncharacterized defects may be the main cause for the degradation of thin gate oxides. Thus an understanding of the hydrogen chemistry in gate oxides is of utmost importance for the further downscaling of semiconductor devices.

In a previous paper[6] we have traced the origin of the SILC back to two defects. That work was based on an extensive investigation of defects in oxides. The defects investigated were interstitial hydrogen, oxygen vacancies and their complexes with hydrogen, their charge states and metastable partners. Here I provide a fuller account of the results, including energetic and structural information on the defects. Furthermore I have calculated charge-state levels, which define the stable charge states as a function of the Fermi level and which determine electron transport. Transition-state structures and activation energies for the transitions between metastable configurations of the defects are presented in order to understand their interconversion process. Finally I give our calculated hyperfine parameters, which exhibit unprecedented accuracy and which furthermore allow me to comment on some problems of the underlying theory.

Section II describes the computational setup, defines reference energies, introduces the defect notation, and provides an overview of the systems investigated. Sections III–VII describe the individual defects in the context of previous experimental and theoretical findings. A brief summary is given in Sec. VIII.

II. METHODS

The calculations presented here are based on density-functional theory (DFT),[7] using gradient corrections.[8,9] Total energies and structures are calculated using the projector augmented wave (PAW) method.[10] As an all-electron method, PAW allows the calculation of hyperfine parameters directly from the all-electron spin density, which allows our structures to be confirmed by comparing them with experiment. One *s* projector has been used for hydrogen, two *s* and two *p* projectors for oxygen, and for silicon an additional *d*-projector function has been introduced. The wave functions have been expanded up to a plane-wave cutoff of 30 Ry and the density up to 60 Ry.[11]

The calculations presented here were done in α quartz. I used a tetragonal supercell containing 24 SiO_2 formula units and having lattice constants of $(a,b,c)=(8.59,9.82,10.80)$ Å.[12,13] A crystalline matrix was chosen because it is a well-defined reference system for the evaluation of relative energies, thus avoiding sampling over a large number of different sites. It should be kept in mind that the oxide near the interface is strained, and that the amorphous matrix itself imposes a compressive or tensile strain on individual bonds.

Energies are calculated with respect to a reservoir of elemental silicon, α quartz, and the interstitial hydrogen molecule in α quartz. This choice is motivated on the one hand by the fact that silica can exchange oxygen atoms with silicon by moving its phase boundary. On the other hand I have used the interstitial hydrogen molecule, as it is the most stable form of hydrogen in silica in the absence of other structural defects. The chemical potential of the electron has been chosen at the silicon midgap energy, determined empirically.[6] The absolute reference energies are -108.942 eV for silicon, -442.298 eV for oxygen, -15.239 eV for hydrogen, and 5.438 eV for the electron in silica and 6.355 eV in silicon.

In the following I describe these reference systems and establish the accuracy of the computational setup by comparing the results for related bulk and gas-phase systems with

TABLE I. Energetics of gas phase and bulk energies. E_{tot} is the DFT total energy in the frozen-core approximation, whereas E_{ref} is the sum of reference energies for all atoms described in the text for the respective atoms. Zero-point corrections are not included. The Si-midgap energy $E_F[\mathrm{Si}]$ has been obtained by adding half the experimental band gap (0.57 eV) to the Kohn-Sham valence band top. $E_F[\mathrm{SiO_2}]$ has been chosen 0.2 eV below the thermodynamic $+/-$ charge-state level of interstitial hydrogen in silica.

	E_{tot} [H]	$E_{tot}-E_{ref}$ [eV]
$O[G]$	−15.98795	7.243
$O_2[G]$	−32.19721	8.465
$H[G]$	−0.49846	1.675
$H_2[G]$	−1.16581	−1.245
$Si[G]$	−3.83876	4.484
$Si_8[X]$	−31.99876	0.806
$Si_{64}[X]$	−256.22706	0.000
$(SiO_2)_{24}$	−876.28376	0.000
$(SiO_2)_{24}H_2$	−877.39827	0.000
$Si_{64}(\Gamma)$	−255.99013	6.447
$Si_{64}H_2(\Gamma)$	−257.11449	6.330
$Si_{64}H^+(\Gamma)$	−256.74943	7.380
$\epsilon_F[\mathrm{SiO_2}]$	0.19986	0.000
$\epsilon_F[\mathrm{Si}](\Gamma)$	0.23354	0.000
$\epsilon_F[\mathrm{Si}](4k)$	0.23186	−0.046

accurate values from the literature.

Our quartz structure exhibits bond lengths of 1.623 and 1.628 Å , respectively. The bond lengths are 1% longer than experiment[13] and agree with previous calculations[15] within 0.1%. Our bond angle is 2° smaller than experiment,[13] which results from the slight expansion in the bond lengths compared to experiment. The asymmetry between short and long bonds, 0.3%, is close to the experimental value of 0.5%.[13] The cohesive energy per molecular unit is 18.97 eV, which is in good agreement with the experimentally determined value of 19.23 eV.[16] Our gradient-corrected results underbind experiment by 0.1 eV/atom; calculations without gradient corrections[17] overbind silica by 1 eV per atom.

The chemical potential for electrons is chosen as the silicon midgap energy at the Si-SiO_2 interface, that is 3.87 eV above the Kohn-Sham valence band edge of quartz. It should be noted that the Kohn-Sham equations yield considerably incorrect band edges. For example the Kohn-Sham band gap of silica is 5.757 eV, which is substantially lower than the true band gap of about 9 eV.[18–22] The relative position of the calculated and experimental band edges is discussed in detail in Sec. V.

The reference calculation for silicon has been done in a 64-atom supercell using four k points. This calculation corresponds to a 256-atom supercell with Γ-point sampling. The Si lattice constant was taken to be 5.43 Å . The atomization energy of silicon is 4.48 eV without considering zero-point vibrational corrections, which compares well with the experimental cohesive energy of 4.63 eV.[23] A smaller calculation equivalent to 64 atoms with Γ-point sampling yielded energies that were 0.1 eV higher per atom, as shown in Table I.

I have calculated the energy to transfer a hydrogen molecule from the vacuum into the silicon crystal as 1.13 eV (Ref. 24). This result compares well with that of Van de Walle, who obtained 0.8 eV.[25] The remaining discrepancy can probably be attributed to the use of different functionals, namely the inclusion of gradient-corrected functionals in the present work. Gradient corrections are extremely sensitive to the change in surface area during a reaction. Therefore one may get an order of magnitude estimate from the atomization energy of a hydrogen molecule. The gradient correction destabilizes the hydrogen molecule by 0.35 eV (Ref. 9) compared to purely local functionals, in good agreement with the discrepancy found here.

Hence hydrogen molecules are 0.12 eV more stable in silicon than in quartz, where the energy to introduce a hydrogen molecule is 1.24 eV. Hydrogen molecules in silicon may serve as alternative reservoir for hydrogen near the interface if the hydrogen concentration in silicon is known. Note that the binding energy in silica is *smaller* than that in silicon, but this may be different in amorphous silica owing to the variations in cage sizes.

The energy required to split a hydrogen molecule in silicon into two interstitial protons is 0.99 eV per atom, which is, as will be shown below, close to the energy of an interstitial proton in silica. The binding energy of the hydrogen molecule is 4.338 eV, including the zero-point vibration energy of 0.257 eV,[26] which compares well with the Becke-Perdew-Wang result of 4.341 eV (Ref. 27) as well as with the experimental value of 4.488 eV.[27]

The binding energy of an oxygen molecule is calculated to be 5.912 eV, including the zero-point vibration energy of 0.110 eV,[26] which is comparable to the atomization energy of 5.906 eV,[27] obtained with the Becke-Perdew-Wang gradient-corrected density functional. At 5.116 eV, the experimental binding energy is substantially smaller (by 0.795 eV) than the theoretical prediction.

In this work, emphasis is placed on charge-state transitions of the defects. We have to differentiate between the thermodynamic charge-state levels ϵ_{th} and the switching charge-state levels ϵ_{sw}.[28] A thermodynamic charge-state level corresponds to the Fermi-level position for which a defect changes its charge state in thermal equilibrium. It is obtained as the energy difference $\epsilon_{th}=E(N+1)-E(N)$ of two charge states, where each is in the structure of its own ground state. The energy required to move, for example, an electron from the reservoir into an unoccupied charge-state level is $\epsilon_{th}-\epsilon_F$, where the thermodynamic charge-state level is the energy require to add an electron and the Fermi level ϵ_F is the energy required to remove an electron from the reservoir. Electrical measurements and electron transport processes, however, are fast compared to the thermal approach to equilibrium. Hence I define switching levels as the electron or hole energy required either to charge or to uncharge a defect in a tunneling process consistent with the Frank-Condon principle, i.e., without allowing any relaxation of the atomic structure. These levels are obtained from the total energy difference of two charge states in the structure of one charge state. Hence the direction of the charging process matters: For example, the $0/-$ level denotes the energy required to add an electron to the neutral defect, and the $-/0$ level denotes the energy of the electron when it leaves the negative charge state. The $0/-$ level obtained is $\epsilon_{sw}(0/-)=E(-)-E(0)$ in the atomic structure of the neu-

TABLE II. Properties of isotopes with nonzero spin and conversion factors (Ref. 31). S is the nuclear spin, M the magnetic moment, ΔB the hyperfine splitting, and B^N the magnetic field of the electron spin at the nuclear site. $\mu_N = 5.050\,787 \times 10^{-27}$ J/T is the nuclear magneton.

Nucleus	Nat. abundance	$S\,[\hbar]$	$M\,[\mu_N]$	$\Delta B/B^N \times 10^3$
e		1/2	1838.28	
^{1}H	99.985%	1/2	2.79284	3.04206
^{17}O	0.05%	5/2	−1.8938	−0.412558
^{29}Si	4.67%	1/2	−0.5553	−0.604844

tral charge state, whereas the $-/0$ switching level is obtained by the same expression using the structure of the negative charge state.

There is a chemical analogy between charge-state levels and reaction events. The reaction in this case is the transfer of an electron to or from the reservoir. Like a reaction free energy, the thermodynamic charge-state level determines the concentration of charge defects in thermal equilibrium. The switching charge-state level on the other hand corresponds to the activation energy for that reaction.

For charged systems a charge-compensating background has been automatically added. Except when stated otherwise, our numbers have not been corrected for the interaction of the charged defect with the compensating background or its periodic images. A conservative estimate of the error can be obtained from a simple model[29] in which the unit cell is approximated by a sphere of equal volume, and the charged defect by a point charge in the center of the sphere. By comparing this system with the energy of an isolated point charge, an estimate of the electrostatic interaction between the periodic images is obtained. The unperturbed silica is described by a dielectric with a dielectric constant of $\epsilon_r = 4.48$.[14] The sphere radius is $r_c = 6.01$ Å . The total energy of a point charge with total charge $-N$, interacting with the positive charge background and the self-interaction of the compensating background, yields $\Delta E = 9N^2/(10\epsilon_r r_c)$, which should be added to our energies. For singly charged defects the correction predicts energies to be higher by $\Delta E = 0.48$ eV, which is to be taken as an error bar on our calculated energies.

Energy levels are affected such that our calculated $0/-$ and $-/0$ levels need to be corrected upward by 0.48 eV, and the $+/0$ and $0/+$ levels downward by the same amount. The relaxation energies of switching levels, i.e., $\epsilon_{0/-} - \epsilon_{-/0}$ and $\epsilon_{+/0} - \epsilon_{0/+}$, are unaffected by the correction. Similarly the $+/-$ levels are not affected by the background.

Hyperfine parameters result from the interaction between the nuclear spin with the electron-spin distribution,

$$E = \sum_{i,j} S_i^e A_{i,j} S_j^N, \tag{1}$$

where S_i^e are the components of the electron spin and S_j^N those of the nuclear spin. The hyperfine coupling constant $\mathbf{A}$ is given by

$$A_{i,j} = \frac{|M^e||M^N|}{|S^e||S^N|}\left(\frac{2\mu_0}{3}\delta_{i,j}\int dr\,\delta_T(r) n_s(r) + \frac{\mu_0}{4\pi}\int d^3r \frac{n_s(r)}{r^3}\,\frac{3r_i r_j - \delta_{i,j}\mathbf{r}^2}{r^2}\right), \tag{2}$$

where the electron coordinate r is taken relative to the position of the nucleus, and M^e and M^N are the electronic and the nuclear magnetic moment.[30] $\delta_T(r)$ is a smeared out δ function as described in the Appendix. $n_s(r) = n_\uparrow - n_\downarrow$ is the difference density of spin-up and spin-down electrons at r, and μ_0 the permeability of vacuum. The values for the magnetic moments M^e, M^N for electrons and nuclei and their spin quantum numbers S^e, and S^N are provided in Table II. The isotropic component or Fermi-contact term $a = \frac{1}{3}\mathrm{Tr}[\mathbf{A}]$ is sensitive only to the density of s electrons at the nucleus. The anisotropic term $A_{i,j} - a\,\delta_{i,j}$ is sensitive to the $l=2$ component of the density near the nucleus which is determined by the p contribution of the wave function in the absence of any d orbitals. Therefore the hyperfine parameter provides direct insight into the electron distribution or wave function near the corresponding nucleus, and thus its hybridization. The hydrogen hyperfine parameters are clearly observable because of the large natural abundance of hydrogen nuclei with nonzero spin. The oxygen hyperfine parameters are not presented in this work because they can only be observed in isotopically enriched samples (see Table II).

Hyperfine splittings refer to the energy difference ΔE in microwave absorption lines. It reflects the magnetic interaction of the nuclear spin with the electronic spin distribution. The splitting is frequently expressed as the change of the effective nuclear magnetic field acting on the electron, $\Delta B = \Delta E/(g_e \mu_B)$, when the nuclear spin changes its component parallel to the electron spin by $\hbar$. Here g_e is the g factor of the free electron and μ_B is the Bohr magneton. In this paper hyperfine parameters are given in units of 1 mT = 10 G = 10 O. Often the splitting is also provided as the microwave frequency $\nu = \Delta E/(2\pi\hbar)$, the conversion being $\nu[\mathrm{MHz}] = 28.024\,95\,\Delta B[\mathrm{mT}]$. Earlier papers also use the notation of megacycles per second, defined as 1 Mc/s = 1 MHz, whereas one only rarely finds data in wave numbers $(1/l)[\mathrm{cm}^{-1}] = 0.934\,811 \times 10^{-3}\,\Delta B[\mathrm{mT}]$. It should be noted that often the electron g factor is approximated by 2, which causes differences of 0.1%.

The notation of the axes of the hyperfine parameters used in this paper is borrowed from Isoya, Weil, and Halliburton,[32] The direction is given by a pair of angles (θ, φ). The polar angle θ is the angle from the c axis, and the azimuthal angle is measured from a lattice vector perpendicular to the c axis. The direction of the z axis has been chosen such that the bonds wind counterclockwise around the large channels in the direction of the positive z axis. There are two forms of α quartz, right and left quartz, which are enantiomers. Our data are based on right quartz. Defect-free silica consists of a network of silicon atoms connected via four oxygen bridges to other silicon atoms.[33] Hence ev-

ery silicon has four bonds to oxygen, and every oxygen is bound to two silicon neighbors. The silicon atoms form rather stiff tetrahedra with their four oxygen neighbors.[34,35] These tetrahedra have a silicon atom in their center and the four oxygen atoms at the corners. They are connected via their corners to neighboring tetrahedra, so that every oxygen atom is shared between two tetrahedra.

Defects in the short-range structure of silica can be classified according to rather general structural motifs, namely under- and overcoordinated atoms and incorrect bonds. A defect notation[36] that describes the atom by its element symbol, followed by its coordination in parentheses, will be used. For example, a [Si(3)] atom describes a silicon atom with one dangling bond and three bonds to oxygen atoms. For correctly coordinated atoms such as [Si(4)] and [O(2)], the coordination number is usually dropped. Incorrect bonds are represented by the ill-coordinated cluster. For example, $[\mathrm{SiSi}(5)^{-}]$ denotes a fourfold-coordinated silicon atom bound to a silicon atom that itself is coordinated to another four oxygen atoms. This defect is in the negative charge state.

For the description of the long-range order the ring size is widely used. A ring is denoted by the number of silicon atoms it contains. Typical ring sizes in silica range from four to 8. Quartz consists of six- and eight-membered rings;[37] cristobalite, a high-temperature form, contains only six-membered rings.[37] Vitreous silica contains five-, six-, and seven-membered rings.[38] In zeolites the ring sizes can vary substantially. The strain energies of small rings in silica have recently been estimated by Hamann.[39]

Of the structural parameters I use the tetrahedral distortion t, which is a measure of the hybridization of the silicon atom. A perfect tetrahedron—corresponding to an sp^3 hybridized atom—has a tetrahedral distortion of one, whereas a planar trigonal structure—corresponding to sp^2 hybridization—has a zero tetrahedral distortion. The tetrahedral distortion is defined via the sum of the angles of three bonds. A total angle of 360° corresponds to a planar sp^2 configuration, and a total angle of 328.5° corresponds to a tetrahedral sp^3 configuration. The tetrahedral distortion is then defined as $t=(360-\Sigma_{i=1,3}\alpha_i)/31.5$.

Defects related to silicon dangling bonds are classified according to a notation that refers to the electron spin resonance (ESR) signal.[40] The notation E' stands for electron excess center as suggested by ESR results, i.e., a defect containing one trapped electron. Defects with more or fewer than one trapped electron are denoted by the number of primes, i.e., a E'' center denotes a defect with two trapped electrons. Numeral subscripts refer to defects in α quartz, whereas Greek subscripts refer to defects in amorphous silica.

I differentiate between the two silicon atoms that participate in the oxygen vacancy. The atom at the long-bond side is called $\mathrm{Si}_{(1)}$ and the one at the short-bond side is called $\mathrm{Si}_{(2)}$. The $\mathrm{Si}_{(2)}$ atom will rebond in the metastable oxygen vacancy with an oxygen bridge.

The defects investigated can be grouped into four classes. The first class are defects related to the isolated oxygen vacancy, which can be divided into two subgroups. One is related to a missing oxygen and its charge states and the other, which contains the well-known E'_γ center, results from a reconstruction in which a bond that formerly pointed into the vacancy has now reversed its direction. The second class is related to the hydrogen atom and its charge states. The third class is related to a hydrogen atom in an oxygen vacancy. Analogous to the oxygen vacancy, the hydrogenated oxygen vacancy is divided into two subgroups depending on the direction of the rebonding. The fourth group corresponds to an oxygen-vacancy complex with two hydrogen atoms.

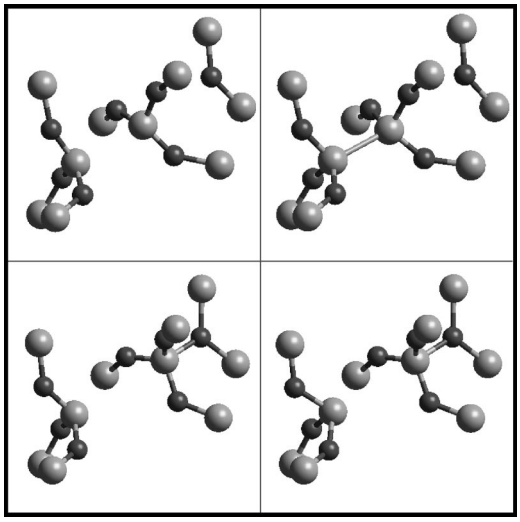

FIG. 1. Structures of the oxygen vacancy. Top left: $[\mathrm{SiSi}^{+}]$ or E'_δ center; top right: [SiSi], the stable configuration of the oxygen vacancy; bottom left: $[\mathrm{Si}(3)+\mathrm{O}(3)^{+}]$ or E'_γ center; bottom right: $[\mathrm{Si}(3)^{-}+\mathrm{O}(3)^{+}]$.

I have excluded from this study defects that involve oxygen levels. The charge-state levels of oxygen hole centers lie in or close to the valence band of the oxide, from which they are derived. Thus they cannot be depleted of electrons as long as the Fermi level is close to the Fermi level of the metal gate or within the band gap of the silicon. Oxygen-hole centers may, however, play an important role as hole traps, a process that is not considered here.

Similarly I have excluded the hydroxyl groups [OH] (Ref. 41) and the [SiH] fragment, except for the dihydrogen complex with an oxygen vacancy. These two defects can be regarded as rather inert and electrically inactive defects in silica, but both are probably abundant owing to their stability, and may play a crucial role in the breakdown of gate oxides as a supply of hydrogen, which ultimately is believed to do the damage. These defects shall be considered in a future study.

III. OXYGEN VACANCY

The oxygen vacancy exists in two different structural conformations,[42–44] each of which has a positive and a neutral charge state (see Fig. 1). In the conformation [SiSi], an oxygen atom is removed and the silicon dangling bonds combine to form a direct silicon-silicon bond. This defect is the stable configuration of the oxygen vacancy. It has a filled state in the lower part of the oxide band gap, as seen from the switching levels in Fig. 2 and in Table III.

If an electron is removed, the positive charge state $[\mathrm{SiSi}^{+}]$ is obtained, which has been identified with the E'_δ center in amorphous silicon.[45–47] Compared to the neutral

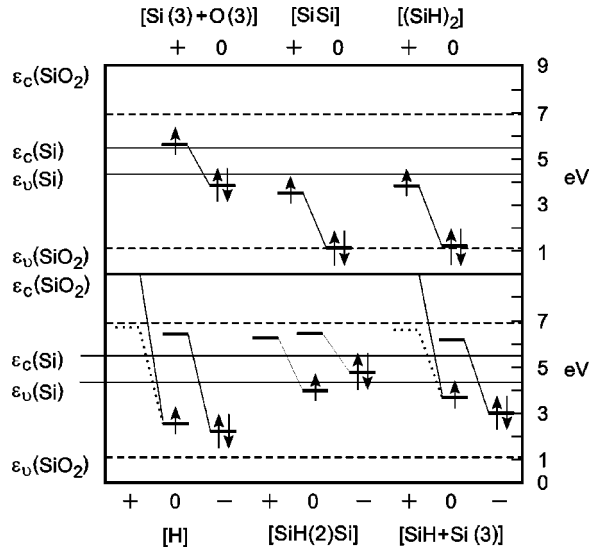

FIG. 2. Switching charge-state levels.

charge state, the bond of $[SiSi^+]$ is weakened, as is evident from the elongation shown in Table IV.

One of the ''dangling bonds'' in the positive charge state can reverse its direction after overcoming a barrier of 0.38 eV (see Tables V and VI), and bind to an oxygen bridge. This configuration is referred to as $[Si(3)+O(3)^+]$, i.e., a pair consisting of a silicon dangling bond and an overcoordinated oxygen atom. Its defect has been identified with the E_1' center, which is called the E_γ' center in an amorphous matrix. The E_1' center has been studied extensively, both experimentally[40,48–53] and theoretically.[42–44,47,54–60]

Adding a second electron to the dangling bond creates an ion-pair complex $[Si(3)^-+O(3)^+]$ with a positive charge on the overcoordinated oxygen atom and a negative charge on the lone pair at the undercoordinated silicon atom. This defect is metastable and transforms into the neutral oxygen vacancy [SiSi] after overcoming a small barrier. I have not evaluated the barrier, but observed in a dynamical simulation starting from the structure of the positive charge state that the barrier is overcome spontaneously, indicative that the barrier is overcome immediately after the electron-capturing process. This reaction is strongly exothermic with nearly 3 eV (see Table VII).

The neutral silicon bond is the thermodynamically stable configuration of the oxygen vacancy for reasonable positions of the Fermi level, see Fig. 3 and Table III. Typically the Fermi level in the oxide is determined by the Fermi levels of the contacts, which lie just above the silicon midgap energy.[61] For bulk oxides, the Fermi level may be determined by the charge neutrality condition of defects. As we will see, hydrogen-related defects, which can be considered abundant in many oxides, also have charge-state levels in a small energy window near the silicon band gap, which may cause Fermi-level pinning in bulk oxides at a position close to the silicon midgap energy at the interface.

As can be seen in Fig. 3 and Table III, the positive vacancy is stable only for Fermi levels that lie nearly 3.0 eV below the silicon midgap energy, which is the energy required to lift an electron from the filled orbital of the neutral oxygen vacancy to the silicon midgap energy. Hence the oxygen vacancy remains in the neutral charge state, unless activated by irradiation or avalanche hole injection, where it acts as a deep hole trap. This casts some doubt on the importance of the undecorated oxygen vacancies [SiSi] and $[Si(3)+O(3)^+]$ for the electrical device properties.[62] The positive oxygen vacancy in the configuration $[Si(3)+O(3)^+]$ can be created by irradiation followed by a ther-

TABLE III. Thermodynamic and switching charge-state levels. Levels are in eV relative to the silicon midgap, and lower bounds are given when shallow donor levels are involved. Numbers without (ϵ) and with (ϵ+corr.) correction for the compensating charge background are provided. See text for details.

		Thermodynamic levels					
		ϵ	ϵ+corr.			ϵ	ϵ+corr.
[SiSi]	+/0	−3.03	−3.51	[SiH(2)Si]	+/0	0.33	−0.15
$[Si(3)+O(3)]$	+/0	−0.06	−0.54		0/−	0.74	1.22
[H]	+/−	0.20	0.20	[SiH+Si(3)]	+/−	0.30	0.30
$[(SiH)_2]$	+/0	−2.74	−3.22				
		Switching levels					
		ϵ	ϵ+corr.			ϵ	ϵ+ corr.
$[SiSi^+]$	+/0	−1.38	−1.86	$[Si(3)+O(3)^+]$	+/0	+0.68	0.20
$[SiSi^0]$	0/+	−3.70	−4.18	$[Si(3)^-+O(3)^+]$	0/+	−1.02	−1.50
$[O(3)^+H]$	+/0	>+1.84	>+1.36	$[SiH+O(3)^+]$	+/0	>+1.71	>+1.23
$[H^0]$	0/+	−2.26	−2.74	[SiH+Si(3)]	0/+	−1.21	−1.88
	0/−	+1.54	+2.02		0/−	+1.27	+1.75
$[Si(5)^-H]$	−/0	−2.70	−2.22	$[SiH+SiSi(5)^-]$	−/0	−1.85	−1.37
$[SiH(2)Si^+]$	+/0	+1.37	+0.89	$[(SiH)_2^+]$	+/0	−1.07	−1.55
[SiH(2)Si]	0/+	−0.85	−1.33	$[(SiH)_2^0]$	0/+	−3.67	−4.15
	0/−	+1.58	+2.05				
$[SiH(2)Si^-]$	−/0	−0.13	+0.35				

TABLE IV. Structure of the oxygen vacancies [SiSi] and [$SiSi^+$].

	[$SiSi^+$]	[SiSi]
$d(Si_{(1)}\text{-}Si_{(2)})$	3.011Å	2.445Å
$d(Si_{(2)}\text{-}O(3)^+)$	3.554Å	3.893Å
$d(Si_{(1)}\text{-}O)$	1.600Å	1.642Å
$d(Si_{(2)}\text{-}O)$	1.597Å	1.641Å
$t[Si_{(1)}]$	0.610	1.298
$t[Si_{(2)}]$	0.483	1.257

TABLE VI. Structural parameters of the transition state for the conversion of the positive oxygen vacancy.

	[$SiSi^+$]↔[$Si(3)+O(3)^+$]
$d(Si_{(1)}\text{-}Si_{(2)})$	3.733Å
$t[Si_{(1)}]$	0.994
$t[Si_{(2)}]$	0.029
$d(Si_{(2)}\text{-}O(3))$	2.567Å
$d(Si_{(1)}\text{-}O)$	1.632Å
$d(Si_{(2)}\text{-}O)$	1.573Å

mal anneal.[52] Irradiation creates the positive oxygen vacancy [$SiSi^+$], which is converted by the thermal anneal into the metastable [$Si(3)+O(3)^+$].

The [$SiSi^+$] and the [$Si(3)+O(3)^+$] defects are nearly isoenergetic, with the [$SiSi^+$] slightly less stable by 0.04 eV. The barrier has been calculated to be 0.38 eV, in agreement with Boero *et al.*[44] Previous calculations,[44] however, predicted that [$Si(3)+O(3)^+$] would be more stable by 0.3 eV. I attribute this discrepancy to the overbinding of the SiO bond in local density approximation (LDA),[63] as opposed to the gradient-corrected functionals used in the present study. My fixed-point calculations using only local exchange and correlation[8] give the [$Si(3)+O(3)^+$] defect as being 0.18 eV more stable, in sufficient agreement with the previous result.

Quantum chemical cluster calculations[47] predict that [$SiSi^+$] is less stable than [$Si(3)+O(3)^+$] by 0.64 eV with a barrier of 0.38 eV for the transition to [$Si(3)+O(3)^+$]. Their structures differ considerably from our calculations, possibly due to the use of the Hartree-Fock method for geometry optimization.

From the barrier of 0.38 eV for the transition between [$SiSi^+$] and [$Si(3)+O(3)^+$], I estimate a rate of 10^6 s^{-1} $\approx 10^{14}$ $s\times\exp(-E_A/k_BT)$ for the conversion at room temperature. Hence one would expect to see both configurations in about equal concentrations, whereas in isochronal annealing studies the E'_γ center apparently anneals at much higher temperatures than E'_δ.[45] Thus there is still an open issue related to the apparent higher stability of the E'_γ center compared to the E'_δ center in the isochronal annealing experiments. One explanation is that the concentration measured in isochronal annealing experiments does not only reflect thermal stability, but also the charge-transfer process that makes the defect EPR invisible. As the charging level of E'_δ lies at lower energies it may be decharged earlier as the effective Fermi level rises during the isochronal anneal. In this scenario E'_δ and E'_γ are in thermal equilibrium at higher temperatures. During cooling, the relative concentrations would be frozen in, but the E'_δ centers would disappear as they are converted to neutral oxygen vacancies. The charging level of the E'_δ center lies 1.38 eV below the silicon midgap, where it can capture electrons from other filled defect states or the contacts. In contrast, the charging level of the E'_γ center lies 0.68 eV above it, which explains the stability of the latter against decharging. At present we must regard this explanation as speculation because more work is required to understand the isochronal annealing experiments. Experiments that vary anneal times and quench rates may shed light on this problem.

TABLE V. Activation energies $E^\ddagger$ and reaction energies ΔE for transitions among defects. The arrow points in the exothermic direction. Energies are in eV.

Transition	$E^\ddagger$	ΔE
[$SiSi^+$] → [$Si(3)+O(3)^+$]	0.344	0.038
[$SiH+Si(3)$]→[$SiH(2)Si$]	0.894	0.157
[$SiH(2)Si^+$]→[$SiH+O(3)^+$]	0.262	0.055

The number of oxygen vacancies at the interface with silicon is determined by the equilibrium with the position of the Si/SiO_2 interface via the reaction

$$\frac{1}{2}Si_X \rightarrow \frac{1}{2}SiO_2 + [SiSi], \tag{3}$$

i.e., an oxygen atom is transferred across the interface into the silicon, oxidizing it to SiO_2. Left behind is an oxygen vacancy [SiSi] in SiO_2. The formation energy of oxygen vacancies of 0.90 eV corresponds to an equilibrium concentration of 1.5×10^{19} cm^{-3} at typical annealing temperatures of 1000 °C, obtained from the density of 5×10^{22} cm^{-3} oxygen sites and the exponential factor of 2.7×10^{-4}, or 1 vacancy per 3600 oxygen sites.

This estimate is two orders of magnitude larger than the measured concentration of 4×10^{17}-cm^{-3} E' centers at the interface to silicon in thermal oxides irradiated with a 5-eV excimer laser[64] and with 2×10^{17} cm^{-3} at γ-irradiated thermal oxide.[65] The experiment of Fiori and Devine[64] assumes a constant concentration of E' centers over a 2500-Å thermal oxide. Marquardt and Sigel,[65] on the other hand, obtain a

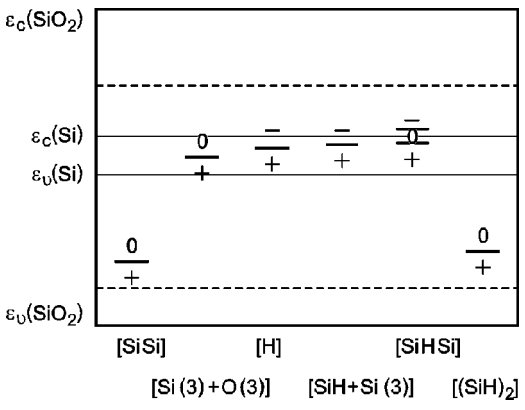

FIG. 3. Thermodynamic charge-state levels.

TABLE VII. Total energies (in eV) relative to the reservoir energies described in the text. Superscripts with two charge states separated by a slash indicate that the structure is obtained from the first and the electron occupation from the second charge state. To obtain energies for Fermi-level positions other than the estimated silicon midgap position, add the deviation of the Fermi level for positive charge states and subtract it for negative charge states. The energies denoted as E are obtained without, those denoted as $E+\text{corr.}$ with correction for the compensating charge background. See text for notation and reservoir energies.

System	E	$E+\text{corr.}$	System	E	$E+\text{corr.}$	System	E	$E+\text{corr.}$
[SiSi]	0.90	0.90	[Si(3)+O(3)]	3.84	3.84	$[(SiH)_2]$	−0.14	−0.14
$[SiSi^{0/+}]$	4.61	5.09	$[Si(3)+O(3)^{0/+}]$	4.86	5.34	$[(SiH)_2^{0/+}]$	3.53	4.01
$[SiSi^{+/0}]$	2.56	2.56	$[Si(3)+O(3)^{+/0}]$	4.58	4.58	$[(SiH)_2^{+/0}]$	1.54	1.54
$[SiSi^{+}]$	3.94	4.46	$[Si(3)+O(3)^{+}]$	3.90	4.38	$[(SiH)_2^{+}]$	2.61	3.09
$[Si(5)H^{-}]$	1.45	1.93	$[SiH+SiSi(5)^{-}]$	1.86	2.34	$[SiH(2)Si^{-}]$	2.47	2.95
$[Si(5)H^{-/0}]$	4.14	4.14	$[SiH+SiSi(5)^{-/0}]$	3.70	3.70	$[SiH(2)Si^{-/0}]$	2.61	2.61
$[H(0)^{0/-}]$	3.86	4.34	$[SiH+Si(3)^{0/-}]$	3.15	3.63	$[SiH(2)Si^{0/-}]$	3.31	3.79
$[H(0)^{0}]$	2.32	2.32	[SiH+Si(3)]	1.89	1.89	[SiH(2)Si]	1.74	1.74
$[H(0)^{0/+}]$	4.58	5.06	$[SiH+Si(3)^{0/+}]$	3.09	3.57	$[SiH(2)Si^{0/+}]$	2.58	3.06
$[O(3)H^{+/0}]$	2.88	2.88	$[SiH+O(3)^{+/0}]$	2.97	2.97	$[SiH(2)Si^{+/0}]$	2.78	2.78
$[O(3)H^{+}]$	1.05	1.53	$[SiH+O(3)^{+}]$	1.25	1.73	$[SiH(2)Si^{+}]$	1.31	1.79
$[H_2]$	0.00	0.00	[Si(3)+Si(3)]	5.06	5.06			

profile with strongly enhanced concentration near the interface. Thus I extrapolate the results of Fiori and Devine to 10^{18}-cm^{-3} vacancies near the interface. The number of E' centers is furthermore considered a lower bound to the number of oxygen vacancies, as some of the centers may have annealed out during the experiment as mentioned by Fiori and Devine,[64] which may account for the remaining discrepancy between theory and experiment.

A formation energy of 1.1–1.3 eV would have to be assumed to obtain vacancy concentrations in the range of that of the observed E' centers. An error of 0.2–0.4 eV is larger than expected from the inherent errors of the calculation, but a correction of this order can be attributed to the different formation energies in quartz and the amorphous silica on the one hand and experimental uncertainties on the other hand.

Let us estimate the vacancy concentration at the surface in thermal equilibrium with a given partial pressure of oxygen molecules corresponding to the reaction

$$SiO_2 \rightarrow SiO_2 + \frac{1}{2}O_2 + [SiSi] \tag{4}$$

taking place at the surface, i.e., two oxygen atoms can form an O_2 molecule, which is released into the gas phase, leaving behind an oxygen vacancy for each oxygen atom emitted.

The concentration of oxygen vacancies at the surface is estimated as

$$\rho = \rho^0 \exp\left(-\frac{E([SiSi])+\mu_O}{k_B T}\right) = 6\times 10^4\ \text{cm}^{-3}\sqrt{P[\text{atm}]}, \tag{5}$$

where $\rho_0 = 5\times 10^{22}$ cm^{-3} is the density of oxygen sites in silica, $E([SiSi])=0.90$ eV is the formation energy of an oxygen vacancy in silica, and

$$\mu_O = \frac{1}{2}\left[E(O_2) + k_B T \ln\left(\frac{P\lambda_T^3}{k_B T}\right)\right] = 3.622\ \text{eV} + 0.055\ln[P(\text{atm})]\ \text{eV} \tag{6}$$

is the chemical potential of the oxygen atom in the molecular gas, relative to the reservoirs used. $E(O_2)=9.26$ eV is the total energy of the oxygen molecule relative to the reservoir, and the second term is the ideal gas contribution to the free energy. The energy of the oxygen molecules has been corrected upward by 0.795 eV to account for the density functional error in the binding energy. $\lambda_T = \sqrt{2\pi\hbar^2/(m_{O_2}k_B T)} = 0.122$ Å is the thermal de Broglie wavelength of oxygen molecules at 1000 °C.

Thus for an anneal at 1000 °C and atmospheric pressures, the vacancy concentration at the surface is estimated to be 15 orders of magnitude smaller than that at the interface to silicon. Note however that the vacancy concentration changes if the structure is annealed with the gate electrode, because then the gate material determines the relevant chemical potential for the oxygen vacancies.

The low formation energy of an oxygen vacancy near the interface to silicon, i.e., 0.9 eV, and the much higher formation energy near the surface $E([SiSi])+\mu_O$ explains the concentration profile of E' centers,[65] which exhibits a large concentration near the interface to silicon which rapidly decays towards the surface. It also provides a natural explanation for the formation of suboxides near the interface. The suboxide can be regarded as a form of silica with a large vacancy concentration. Given the large vacancy-formation energy relative to a reservoir of bulk silicon, and considering that silicon can be regarded as a form of silica with stoichiometric oxygen vacancy concentration, a tendency towards vacancy clustering is expected. This clustering increases the oxygen deficiency very close to the interface even above the value predicted from the vacancy-formation energy alone. The formation of sub-oxides near the interface can then be

TABLE VIII. Hyperfine parameters (A in mT) and directions (θ,φ in degrees) of the E'_δ center. Atoms Si($1c$) and Si($2c$) are not shown because their hyperfine parameters are smaller than 0.1 mT. The definition of the angles follows the convention of Isoya, Weil, and Halliburton (Ref. 32) and is described in Sec. II. The average of the three splittings is the isotropic hyperfine parameter. The largest deviation of the hyperfine splitting from the average splitting is the anisotropic hyperfine parameter.

	A	(θ,φ)		A	(θ,φ)
Si(1)	−13.5	(120,232)	Si(2)	−10.0	(129,263)
	−10.8	⊥		−8.0	⊥
	−10.8	⊥		−8.0	⊥
Si(1a)	−0.6	(139,272)	Si(2a)	−0.6	(118,180)
	−0.5	⊥		−0.5	⊥
	−0.5	⊥		−0.5	⊥
Si(1b)	−0.7	(61,264)	Si(2b)	−0.2	(55,227)
	−0.6	⊥		−0.1	⊥
	−0.6	⊥		−0.1	⊥

attributed to the vacancy concentration profile in contact with two different vacancy reservoirs near the interface and the surface. It may be of interest to investigate the binding energies of vacancy pairs in future work.

A. Neutral oxygen vacancy: [SiSi]

In the neutral charge state of the oxygen vacancy the two unbridged silicon atoms form a bond that is only 4% larger than a SiSi bond in elemental silicon. The tetrahedral distortion is larger than unity, which is attributed to the strain of the SiSi bond. The SiO bond lengths of the silicon atoms are only insignificantly (1%) expanded relative to the ideal bulk quartz.

The oxygen vacancy has an electron level in the lower part of the gap corresponding to the $(+/0)$ charge-state level. The corresponding one-particle level has the character of a SiSi bond orbital, with some antibonding admixture of oxygen p orbitals. A second SiSi bond orbital, with bonding character with the O neighbors, is found in the valence band.

B. Positive oxygen vacancy [$SiSi^+$] or E'_δ

In the positive charge state the SiSi bond of the oxygen vacancy expands substantially by 23% to 3.02 Å , comparable to the size (3.07 Å) of an oxygen bridge.[44] The two silicon atoms are inequivalent with a larger (by 0.13) tetrahedral distortion on the short-bond $Si_{(1)}$ atom. This asymmetry is a sign of a more positively charged $Si_{(2)}$ atom. Being more positive eases its transformation via a trigonal planar transition state into the structure of the metastable vacancy configuration [$Si(2)+O(3)^+$]. The reason is that a high-lying silicon p orbital is formed in the transition state, which is unfavorable if that orbital is fully occupied. The SiO bond lengths are contracted by 2–3% compared to the neutral vacancy as a result of the reduced electron number on the silicon atoms.

Hyperfine parameters

The calculated hyperfine parameters shown in Table VIII support the identification of the positive oxygen vacancy as the E'_δ center.[47] The E'_δ center has been related to a 10-mT hyperfine splitting,[45] in perfect agreement with our calculated splittings in the range from 10 to 11 mT, with additional bands at 8 and 13.5 mT. Previously the E'_δ center had been attributed to Cl impurity and a spin distributed over four silicon dangling bonds pointing towards it.[45] Subsequently the E'_δ was observed in Cl-free oxides, and the model was modified to a cluster of four oxygen vacancies.[66] In both models the spin is distributed over four silicon dangling bonds, in order to explain the fourfold reduction of the hyperfine parameter compared to simple dangling-bond defects such as E'_γ. However, there is a simpler explanation involving the isolated oxygen vacancy: The spin density of the positive oxygen vacancy is spread over two nearly identical atoms, explaining a reduction by a factor 2. Another factor of 2 results from the wave function being a bond orbital with an increased probability in between the atoms and consequently a reduced probability at the nuclei. The identification gets further support from isochronal annealing studies,[45] which show that the E'_γ concentration *increases* in the temperature range where the E'_δ concentration falls off, indicating an interconversion of the two centers. Hence the E'_δ center should be related to a simple oxygen vacancy.

The structural asymmetry between the two participating silicon atoms, which is seen in the tetrahedral distortions shown in Table IV, is reflected in the asymmetric hyperfine parameters, with a larger Fermi-contact term at the atom at the short-bond side of the vacancy. This indicates that the short-bond silicon atom is more positive than the long-bond silicon atom by about $0.1e$.

C. Reconstructed positive oxygen vacancy [$Si(3)+O(3)^+$] and E'_1 or E'_γ

The metastable, positive oxygen vacancy, [$Si(3)+O(3)^+$], has been identified with the E'_γ center in amorphous silica and with the E'_1 center as it is called in α quartz.[40,42–44,47–60] Although the first structural model proposed by Feigl, Fowler, and Yip[54] suggested a combination of two undercoordinated silicon atoms of which one is posi-

TABLE IX. Structure of the reconstructed oxygen vacancies $[Si(3)+O(3)^+]$ and $[Si(3)^-+O(3)^+]$.

	$[Si(3)+O(3)^+]$	$[Si(3)^-+O(3)^+]$
$d(Si_{(1)}\text{-}Si_{(2)})$	4.358Å	4.052Å
$d[Si_{(2)}\text{-}O(3)]$	1.852Å	1.907Å
$d[O(3)^+\text{-}Si(4)]$	1.793Å	1.784Å
$d(Si_{(1)}\text{-}O)$	1.643Å	1.750Å
$d(Si_{(2)}\text{-}O)$	1.599Å	1.594Å
$t[Si_{(1)}]$	1.098	2.137
$t[Si_{(2)}]$	0.727	0.537

tively charged and in a planar configuration, it is now generally agreed that the positive silicon atom forms a bond with an oxygen bridge, resulting in an overcoordinated, positive oxygen atom as proposed by Rudra and Fowler.[59]

Here the SiSi bond is broken entirely, exposing a singly occupied dangling bond on one silicon atom, whereas the second, more positive silicon switches through the center of its three oxygen nearest neighbors, and binds to an oxygen bridge, resulting in a fourfold-coordinated silicon atom and a threefold-coordinated oxygen atom, which is formally positively charged. With its length of 1.87 Å , the newly formed SiO bond is only 4% longer than the other bonds of length 1.79 Å to the overcoordinated oxygen atom. However, even those bonds are expanded by 10% relative to a normal SiO bond owing to the reduced charge on the oxygen atom, which expands the ionic radius. The details of the structure are provided in Table IX. The results are very close to those obtained previously by Boero *et al.*[44] However, in their calculation the new SiO bond is 3% shorter than in our case, which we attribute to the overbinding of density functionals without gradient corrections used in previous calculations as discussed above.

The $[Si(3)+O(3)^+]$ defect has a silicon-dangling-bond orbital near the the silicon midgap energy, which is split into a spin-up and a spin-down orbital. Interestingly no further gap states related to the threefold-coordinated oxygen have been observed, which explains the tendency of silica to oxide charging. As we will see, this is a general observation of all defects involving threefold-coordinated oxygen atoms.

Hyperfine parameters

Accurate hyperfine parameters of the E_1' center have been measured by Jani, Bossoli, and Halliburton,[52] Our calculated hyperfine parameters shown in Table X exhibit excellent agreement with experiment. Compared to previous pseudopotential calculations by Boero *et al.*,[44] the theoretical prediction of hyperfine parameters has been substantially improved. At this point it is not clear whether this improvement is to be attributed to the more rigorous PAW method, compared to the pseudopotential method combined with a density reconstruction scheme,[67] or to the gradient-corrected density functionals employed in the present work.

As anticipated, the main hyperfine parameter is located on the dangling bond.[44,52] The value obtained is typical for silicon dangling bonds in silica. Only two of the silicon neighbors of the undercoordinated silicon atoms carry sizable hyperfine parameters. This is because the spin density of the dangling bond couples via the *p* orbital on the oxygen bridge to neighboring silicon atoms. The coupling is therefore good if the oxygen bridge lies in the plane perpendicular to the axis of the dangling bond. The third bridge does not fulfill

TABLE X. Hyperfine parameters (A in mT) and directions (θ,φ in degrees) of the E_1' center. Atom Si($1a$) is related to A_1 weak, and Si($1b$) is correlated with A_2 weak. The individual directions of the equatorial components are not defined because of their degeneracy. They are denoted by $\perp$, indicating any vector perpendicular to the axial vector. For the notation of the directions see text.

	This work		Other theory (Ref. 44)		Expt. (Ref. 52)	
	A	(θ,φ)	A	(θ,φ)	A	(θ,φ)
Si(1)	−45.4	(112,233)	51.3	(113,228)	−45.4	(114,230)
	−39.6	$\perp$	44.6	(101,319)	−39.1	(128,340)
	−39.6	$\perp$	44.5	(159,70)	−39.1	(132,116)
Si(1a)	−1.4	(149,281)	2.4	(142,282)	−1.0	(141,285)
	−1.2	$\perp$	1.8	(127,157)	−0.8	
	−1.2	$\perp$	1.8	(119,50)	−0.8	
Si(1b)	−1.5	(59,267)	2.2	(60,253)	−0.9	(59,285)
	−1.3	$\perp$	1.6	(93,169)	−0.8	
	−1.3	$\perp$	1.6	(25,79)	−0.8	
Si(1c)	0.1	(53,193)	0.4	(131,347)		
	0.0	$\perp$	0.4	(100,187)		
	0.0	$\perp$	0.3	(149,83)		
Si(2a)	−0.2	(62,317)				
	−0.1	$\perp$				
	−0.1	$\perp$				

this requirement, and shows clearly reduced hyperfine parameters.[59]

Even smaller hyperfine parameters are found: One of these hyperfine parameters originates from the third silicon neighbor of the undercoordinated silicon. Rather surprisingly I find a hyperfine coupling even on a more distant silicon atom, namely Si($2a$), which is not connected directly to the undercoordinated silicon atom. This atom is part of the strongly strained three ring formed by the additional SiO bond.

D. Reconstructed neutral oxygen vacancy $[\mathbf{Si(3)^- + O(3)^+}]$

The addition of an electron to the $[\mathrm{Si(3)+O(3)^+}]$ defect results in a metastable ion-pair complex with a lone pair on the undercoordinated silicon atom and the positive, overcoordinated oxygen atom.

The main structural relaxation of the neutral $[\mathrm{S(3)^- + O(3)^+}]$ defect relative to the positive charge state is the strong tetrahedral distortion on the undercoordinated silicon atom. Interestingly the tetrahedral distortion on $\mathrm{Si}_{(2)}$ is reduced, indicative of a more positive charge state compared to $[\mathrm{Si(3)+O(3)^+}]$, even though the total electron number is higher. This probably results from a polarization of the undercoordinated oxygen defect due to the presence of a nearby negative charge in the silicon dangling bond.

IV. INTERSTITIAL HYDROGEN MOLECULE

The hydrogen molecule does not react with the defect-free silica lattice. It has no states in the band gap of silica. Thus it may be difficult to activate the hydrogen molecule with UV light in the absence of other defects. This result indicates that hydrogen molecules need to interact with defects in silica before they can be activated.

The hydrogen molecule has four close contacts to oxygen bridges, and two short and two longer close contacts to silicon atoms. These contacts are not to be confused with chemical bonds. The nonbonded interactions are expected to reflect the topology of the channels in α quartz, and may vary substantially in the amorphous material. The energy to introduce a hydrogen molecule into the silica framework is 1.4 eV. The bond length is slightly reduced—by 3%—from 0.766 Å in the gas phase to 0.744 Å in the crystal (see Table XI).

V. INTERSTITIAL HYDROGEN ATOM

Atomic hydrogen in silica has been studied recently by Yokozawa and Miyamoto.[68] The hydrogen atom can exist in three charge states: positive, neutral, and negative. The charged configurations are bonded to the lattice, while the neutral configuration does not bind. The stabilization by bonds to the network is the reason that only the charged modifications are thermodynamically stable for any position of the Fermi level: Hydrogen is a negative-U defect with the $(+/-)$ as its only thermodynamic charge-state level.

The thermodynamic charge-state level of hydrogen has been identified[6] with density of states in the oxide induced either by hydrogen exposure or electric stress as observed by C-V measurements.[69,70] This density of states introduces a characteristic peak 0.2 eV above the silicon midgap energy at the $\mathrm{Si/SiO_2}$ interface. The silicon midgap energy has been defined as the reference for electron energies. This identification has been used to determine the position of the defect states relative to the silicon band gap at the silicon-oxide interface and indirectly relative to the oxide band edges.

Let us now determine the true position of the true band edges relative to our reference energy, the silicon midgap energy at the $\mathrm{Si\text{-}SiO_2}$ interface. The band gap of silicon is $E_G([\mathrm{Si}])=1.14$ eV, and the measured valence band offset between silica and silicon is $\Delta E_V=4.4$ eV.[71,72] As I choose the silicon midgap energy as our reference energy, the true valence band is located at $-E_G/2-\Delta E_V=-5.0$ eV. The band gap of silicon dioxide is 9 eV,[18–22] which locates the conduction band edge of silicon dioxide at $E_C=4.0$ eV.

Using the present functionals, the Kohn-Sham[73] valence band lies at $E_V=-3.88$ eV. This value has been obtained from the energetic position of the thermodynamic charge-state level of hydrogen relative to the Kohn-Sham valence band top, from which 0.2 eV is subtracted because the charge-state level of hydrogen is located by that amount above the silicon midgap energy.[69,70] Using the Kohn-Sham band gap of $E_G=5.76$ eV, the conduction-band edge is located at $E_C=1.88$ eV.

Comparing experiment and Kohn-Sham bands, the Kohn-Sham valence band has to be corrected downward by 1.12 eV, whereas the conduction band has to be corrected upward by 2.12 eV. The overall correction of the band gap is 3 eV.

This empirical determination of the band edges must be regarded with some caution because of the experimental uncertainty of the measured valence-band offset.[74] However, other facts seem to support the identification: (i) As discussed below, the measured optical absorption band of the E_2' center, i.e., [SiH+Si(3)], coincides perfectly with the hole excitation from the dangling bond into the conduction band. (ii) I found it impossible to create self-trapped hole centers that have been observed experimentally.[75] This may be because these states are resonances within the Kohn-Sham valence band as opposed to localized states within the band gap.

The charging behavior of hydrogen is characterized by high relaxation energies of more than 4 eV: >4.1 eV for the $(+/0)$ and 4.24 eV for the $(0/-)$ level. This rules out any involvement of interstitial hydrogen atoms in the stress-induced leakage current. Given that the hydrogen occurs only in charged configurations, electrons can be added only to a shallow donor level at the oxide conduction-band edge, and electrons can be introduced only 2.7 eV below the silicon midgap energy thus, hydrogen acts as hole and electron trap.

In order to probe the total energy surface for positive oxide charging by the presence of neutral atomic hydrogen in

TABLE XI. Structural parameters of the interstitial hydrogen molecule. The parameter d(H-O) is the average over four contacts. The parameter d(H-Si) is divided into two short and two long contacts, where each is the average of two values.

	$[\mathrm{H_2}]$		
d(H-H)	0.744 Å	$d(\mathrm{H\text{-}Si})_{\mathrm{short}}$	2.663 Å
d(H-O)	2.143 Å	$d(\mathrm{H\text{-}Si})_{\mathrm{long}}$	2.875 Å

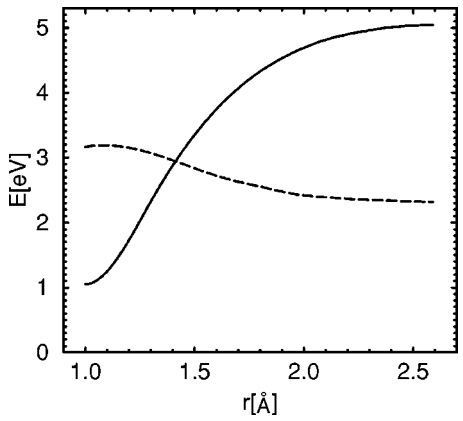

FIG. 4. Energies of positive (solid line) and neutral (dashed line) hydrogen as a function of the distance from an oxygen bridge with the Fermi level at the silicon midgap energy. At different Fermi levels, the energies of the positive hydrogen shift in the same direction as the Fermi level.

more detail, the energetics of the neutral and positive charge states has been investigated as a function of O-H distance, see Fig. 4. These calculations have been performed on a smaller 24-atom cristobalite supercell. The structures have been optimized for neutral hydrogen at a set of fixed O-H distances. For the resulting set of structures I monitored the positive and neutral charge states. The resulting total-energy curves have been shifted to reproduce the calculated energies of the relaxed proton and neutral hydrogen in quartz, respectively, as given in Table VII. Whereas the neutral hydrogen experiences a shallow minimum, the positive charge state is dominated by the strong attraction between the proton and the oxygen bridge. Thus thermal fluctuations of the positions of the neutral hydrogen can be large, and the resulting large variations of the switching charge-state levels, defined as the energy difference between the total energies of the two charge states in a given structure, favor charge transfer, which requires the charge-state levels to cross the Fermi level.

A. Proton: $[O(3)H^+]$

Protons attach spontaneously to an oxygen bridge, forming a threefold-coordinated oxygen atom. As we will see, threefold-coordinated oxygen atoms are a typical structural element of defects in silica. Structural parameters are listed in Table XII.

Protons are not electrically active and do not have one-particle levels in the gap, except a shallow donor level resulting from the Coulomb distortion of the conduction-band edge. Therefore I do not consider the DFT value for the level to be significant and correct it to the estimated conduction-band edge of the oxide. The absence of trap levels for protons is a likely cause of the tendency of silica to positive oxide charging.

TABLE XII. Structural parameters of the positive interstitial hydrogen atom. The bond lengths between oxygen and silicon atoms are averages over two bonds.

	$[O(3)H^+]$
d[H-O(3)]	1.017 Å
d[O(3)-Si]	1.773 Å
∠[Si-O(3)-Si]	134.5°
t [O(3)]	0.165
t(Si)	0.780

TABLE XIII. Structural parameters of the neutral interstitial hydrogen atom.

	[H(0)]
d(H-O)	2.145 Å
$d(\text{H-Si})_{\text{short}}$	2.550 Å
$d(\text{H-Si})_{\text{long}}$	2.880 Å

B. Neutral hydrogen: [H(0)]

Interstitial hydrogen does not form covalent bonds with the lattice. As shown in Table XIII, there are four close contacts to oxygen bridges at about an equal distance of 2.15 Å and two close contacts to silicon atoms each at 2.55 and 2.88 Å .

As shown previously,[68] the interstitial hydrogen atom is a negative-U defect, and the neutral hydrogen is thermodynamically unstable for all positions of the Fermi level. This is confirmed by the observation that the ESR signal related to atomic hydrogen anneals at 190 K.[76,77] Two hydrogen atoms can exchange an electron and form a positive and a negative hydrogen defect. The ion pair $[O(3)^+H]+[Si(5)H^-]$ is more stable by 2.1 or 1.1 eV after correcting for the compensating charge background. The negative-U behavior of hydrogen in silica parallels that in semiconductors.[78]

The neutral hydrogen atom is stabilized by the spin polarization, which results in a large difference between the $0/+$ and the $0/-$ levels, corresponding to a Coulomb repulsion of 3.8 or 4.8 eV after background correction. This large level splitting is the reason that hydrogen, which attaches to the lattice spontaneously after electron capture or loss, is sufficiently stable to be observed in ESR experiments.

Hyperfine parameters

Hydrogen exhibits a clearly distinguishable isotropic hyperfine coupling.[76] The measured hyperfine parameters are slightly smaller in amorphous silica than α quartz, which indicates that hydrogen atoms find larger cages in the amorphous material.

The calculated hyperfine parameters shown in Table XIV agree perfectly with experiment. These values have been obtained with a plane-wave cutoff of 70 Ry. Using 30 Ry underestimates, as expected, the hyperfine parameter by 10%. The sensitivity of hyperfine parameters on basis-set convergence is not unexpected as it is a quantity derived from the density, which unlike the total energy does not profit from a variational principle. Similar observations have been made in calculations of electric-field gradients.[79]

C. Negative hydrogen: $[Si(5)H^-]$

A hydrogen atom in the negative charge state attaches to a silicon atom,[68] making it fivefold-coordinated as shown in

TABLE XIV. Hyperfine parameters of the interstitial hydrogen atom in quartz and the isolated hydrogen atom H[g] (in mT). The value in parentheses was obtained with a plane-wave cutoff of 30 Ry, whereas the other values were obtained with 70 Ry.

H^0	Theory	Expt. (Ref. 76)		Theory	Exact
$H^0[SiO_2]$	50.29 (46.76)	51.91	H[g]	50.93	50.73

Fig. 5. The environment of the silicon atom is that of a distorted trigonal bipyramid with two axial and three equatorial neighbors. In the present calculation the hydrogen atom goes to the equatorial configuration, even though in cristobalite I found the hydride in the axial configuration in agreement with Yokozawa and Miyamoto.[68] The axial SiO bonds are found to be 3.7% longer than the equatorial SiO bonds. The equatorial O-Si-O angle is 14° smaller than the ideal trigonal angle.

The binding results from sp^2 hybridization in the equatorial plane at the silicon atom and a four-electron, three-center bond (see Fig. 6) along the axial direction. The three-center bond involves the axial p orbital on the central silicon atom and lone pairs (dangling bonds occupied with an electron pair) on either side of it. Three orbitals are formed, a fully bonding orbital, a nonbonding orbital with little silicon contribution, and a fully antibonding orbital. The lower two orbitals are occupied with two electrons each. The stabilization is due to the delocalization of the electrons in the former SiO bond orbital over three instead of two sites in the bond orbital. Correspondingly, adding the second bond weakens the former SiO bond, which explains the elongation of the axial bonds as compared to the equatorial bonds seen in Table XV. The nonbonding orbital can contribute to binding only via a next-nearest-neighbor interaction or through admixture of d orbitals on silicon. If the two axial neighbors are identical, no silicon-p contribution will be present in the nonbonding orbital for symmetry reasons. Therefore the bond has been erroneously attributed to Si-d H-s hybridization,[68] which we consider a small effect, compared to the stabilization of the fully bonding orbital in the valence band. Trigonal bipyramidal coordination is a typical structural motif of fivefold-coordinated main group atoms. The negative hydrogen has a fully occupied electron level only 1 eV above the valence-band edge or 1.5 eV after correcting for the background.

VI. HYDROGEN COMPLEX WITH AN OXYGEN VACANCY

Like the bare oxygen vacancy, the complex with a single hydrogen atom also exhibits metastability. There is an analogy between the bare oxygen vacancy and the hydrogenated oxygen vacancy. The stable configuration of the positive hydrogenated oxygen vacancy, $[SiH+O(3)^+]$, corresponds structurally to the E'_γ center $[Si(3)+O(3)^+]$, whereas the oxygen vacancy [SiSi] corresponds to the hydrogen bridge [SiH(2)Si], see Fig. 7. However, in contrast to the oxygen vacancy, the two metastable configurations of the hydrogen complex with the oxygen vacancy have similar energies.

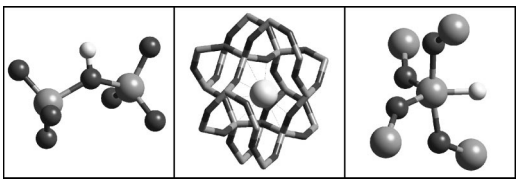

FIG. 5. Structures of the interstitial hydrogen atoms in the positive $[O(3)^+H]$, neutral $[H(0)^0]$ and negative $[Si(5)^-H]$ charge states (from left to right).

The hydrogen bridge [SiH(2)Si] is the simplest complex of a hydrogen atom having an oxygen vacancy. Here, a hydrogen atom enters about midway into the silicon bond. The hydrogen bridge has been attributed to the E'_4 center.[32,49] The hydrogen bridge is qualitatively similar to the position of the neutral interstitial hydrogen in silicon.[80]

The hydrogen bridge has a electron level deep in the band gap. The electronic structure of the hydrogen bridge *is characterized* as a three-center bond between two dangling bond orbitals on the participating silicon atoms and the hydrogen orbital in the center (see Fig. 6). The three-center bond has three orbitals: a fully bonding configuration in the valence band, a fully antibonding orbital in the conduction band, and a nonbonding orbital deep in the band gap. The nonbonding orbital is made up of an antibonding combination of the silicon-dangling-bond orbitals with little admixture of the hydrogen s orbital. This state can also be described as having been *derived* from the antibonding orbital of the SiSi bond of the oxygen vacancy [SiSi]. In the neutral oxygen vacancy [SiSi] it lies in the conduction band, but in [SiHSi] the Coulomb attraction of the proton pulls it into the band gap. As seen in Fig. 8 the hydrogen atom is located near the node plane of the nonbonding orbital.

The nonbonding orbital can be occupied with none, one or two electrons, resulting in the positive, neutral, or the negative charge state of the defect. The antibonding interaction between the silicon-dangling-bond orbitals in the nonbond orbital is weak because the proton results in an expansion of the SiSi bond. On the other hand, the fully bonding orbital in the valence band is always occupied and stabilizes the defect against breaking up. Charging this defect results in only minor structural relaxations, which makes it the prime candidate for the trap responsible for stress-induced leakage currents.[6]

The main relaxation of the hydrogen bridge is an in-

TABLE XV. Structural parameters of negative hydrogen $[Si(5)^-H]$ with the hydrogen in the equatorial position.

	$[Si(5)^-H]$
d [H-Si(5)]	1.508 Å
d[Si(5)-O_{ax}]	1.757 Å
d [Si(5)-O_{eq}]	1.694 Å
$\angle$[O_{ax}-Si(5)-O_{ax}]	170.0°
$\angle$[O_{eq}-Si(5)-O_{eq}]	106.0°

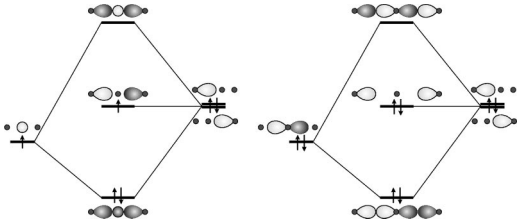

FIG. 6. Orbital scheme of a three-center bond for the example of a central *s* orbital (left) and a central *p* orbital (right). The scheme on the left is a model of the hydrogen bridge [SiHSi]. The scheme on the right is a model of the axial bonds at a fivefold-coordinated silicon atom as in $[\mathrm{Si}(5)^{-}\mathrm{H}]$. The fully bonding orbital is located in the valence band of SiO_2, the fully antibonding one in the conduction band. The middle orbital, which is of nonbonding nature, is located in the SiO_2 band gap.

creased asymmetry with increasing number of electrons. In the positive charge state, the hydrogen is located about midway between the two silicon neighbors. In the negative charge state, the hydrogen behaves like a normal SiH group, and the electrons are localized on the dangling bond of the undercoordinated silicon atom. There are two possible asymmetric relaxations for the hydrogen atom, corresponding to the formation of SiH bonds with either of the two silicon neighbors.[52,58] This is confirmed by the temperature dependence of the hyperfine parameters.[52] In my calculations the two structures are found to be isoenergetic within the accuracy of the method.

The relaxation of 1.7 eV for the neutral-to-negative switching level and 2.2 eV for the positive-to-neutral level are unusually small compared to other defects in silica. Only the thermodynamically unstable oxygen vacancy $[\mathrm{Si}(3)+\mathrm{O}(3)^{+}]$ exhibits similar relaxation energies of 1.7 eV. Thus I conclude that the hydrogen bridge is the prime defect responsible for stress-induced leakage currents.[6]

The prediction provides a natural interpretation of the electrically detected magnetic resonance (EDMR) experiments of the SILC by Stathis,[5] in which a shoulder observed in the spectrum can be explained by no other known defect in silica except the hydrogen bridge. Further confirmation is obtained by measurements by Takagi, Yasuda, and Toriumi,[81] that predict an energy loss of 1.5 eV of SILC. Note, however, that the interpretation of these experiments has recently been called in question.[82] Furthermore, the position of the trap has been estimated as being 1.2–1.8 eV below the oxide conduction band,[83,84] which is in sufficient agreement with our result for a position of the $0/-$ switching level of the hydrogen bridge 2.42 eV below the oxide conduction band. Here I included an estimated correction of 0.48 eV to account for the electrostatic interaction of periodic images in the supercell calculations used as described in Sec. II. Electrical measurements attribute the trap responsible for SILC to a neutral, hydrogen-related electron trap, which is true for the hydrogen bridge.[4]

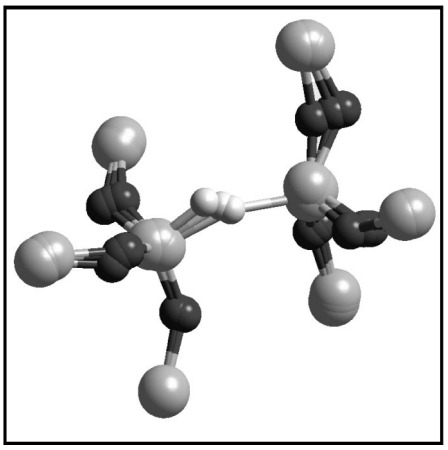

FIG. 7. Structures of three charge states of the hydrogen bridge superimposed. The hydrogen moves further off center with increasing number of electrons. From Ref. 6.

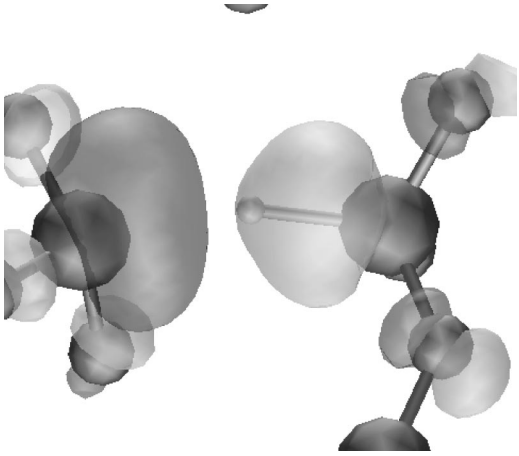

FIG. 8. Highest occupied orbital of the neutral hydrogen bridge.

The second form of a hydrogen complex with a silicon vacancy, [SiH+Si(3)], can be considered a pair consisting of a SiH fragment and an undercoordinated silicon as seen in Fig. 7. As the SiH fragment is relatively inert, this defect is a prototypical silicon-dangling-bond center and may be nearly indistinguishable from the E_s' center. The E_s' center has been attributed to an isolated silicon dangling bond. The [SiH+Si(3)] defect has been attributed to the E_2' center.[40,49,85,86]

There is a close analogy between hydrogen and silicon dangling bonds. Let us use the undercoordinated silicon atom in the [SiH+Si(3)] defect as a typical silicon dangling bond. Like hydrogen, the dangling bond attaches to an oxygen bridge in the positive charge state, forming a threefold-coordinated oxygen atom. The resulting $[\mathrm{SiH}+\mathrm{O}(3)^{+}]$ defect shown in Fig. 9 exhibits no levels in the gap, except for shallow donor levels at the conduction-band edge, which is also true for the positive hydrogen $[\mathrm{O}(3)\mathrm{H}^{+}]$. In the negative charge state the silicon dangling bond attaches to a silicon atom, resulting in an overcoordinated silicon atom in the $[\mathrm{SiH}+\mathrm{SiSi}(5)^{-}]$ defect, see Fig. 9. This is similar to the

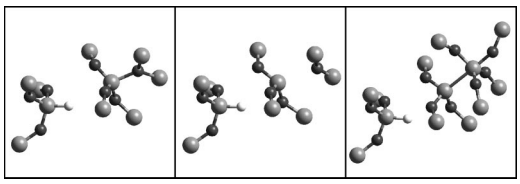

FIG. 9. Structure of the hydrogenated oxygen vacancy in the positive $[\mathrm{SiH}+\mathrm{O}(3)^{+}]$ (left), the neutral [SiH+Si(3)] (middle), and negative $[\mathrm{SiH}+\mathrm{SiSi}(5)^{-}]$ (right) charge state.

TABLE XVI. Structural parameters of the [SiH+Si(3)] defect and its charge states.

	$[SiH+O(3)^{+}]$	[SiH+Si(3)]	$[SiH+SiSi(5)^{-}]$
$d(Si_{(1)}\text{-}H)$	1.477Å	1.460Å	1.467Å
$d(Si_{(2)}\text{-}H)$	3.088Å	2.742Å	3.154Å
$d(Si_{(1)}\text{-}Si_{(2)})$	4.394Å	4.011Å	4.381Å
$t[Si_{(1)}]$	1.057	1.079	1.121
$t[Si_{(2)}]$	0.740	0.997	1.848
$d[Si_{(2)}\text{-}O(3)]$	1.851Å	2.682Å	2.901Å
$d[Si_{(2)}\text{-}Si(5)]$	3.173Å	3.536Å	2.618Å
$d(Si_{(1)}\text{-}O)$	1.636Å	1.633Å	1.633Å
$d(Si_{(2)}\text{-}O)$	1.599Å	1.643Å	1.694Å
$d[Si(5)\text{-}O_{ax}]$			1.750Å
$d[Si(5)\text{-}O_{eq}[$			1.665Å
d[O(3)-Si]	1.796Å		

negative hydrogen atom, which forms a bond with a silicon atom in the $[Si(5)H^{-}]$ defect. If the dangling bond is occupied with only one electron, e.g., in [SiH+Si(3)], it remains unsaturated like the hydrogen *s* level in the neutral charge state [H(0)], and produces a defect level deep in the gap with a well-localized electron density. The levels are split into a spin-up donor level and a spin-down acceptor level.

The rebonding of the charged defects, which is absent in the neutral charge state, results in the negative *U* or small *U*, with $U=0.1$ eV after correction for the charge background, property of the defect, making the neutral charge state thermodynamically unstable for all Fermi-level positions. Interestingly, the thermodynamic $(+/-)$ charge-state levels of hydrogen and [SiH+Si(3)] are separated by only 0.1 eV, and the relaxations of the defect levels upon charging are of similar size. Hence the electrical properties of the hydrogen and the [SiH+Si(3)] defect are expected to be indistinguishable by current-voltage (*C*-*V*) measurements.

The analogy between hydrogen and silicon dangling bonds explains why similar electrical behavior has been observed for electrically stressed gate oxides and hydrogen-free samples, where these effects have been expected to be absent rather than just strongly reduced. For example the nature of the anomalous positive charge, also called border traps or slow states, has been attributed to the oxygen vacancy[87] and hydrogen-related defects.[88] In the absence of hydrogen, however, silicon dangling bonds will exhibit qualitatively similar behavior, although the effects in hydrogen-free samples are limited by the intrinsic concentration of oxygen vacancies.

As seen in Table VII, the defects $[SiH+O(3)^{+}]$ and $[SiH+SiSi(5)^{-}]$ are energetically favored by all charge states of the hydrogen bridge. Hence the oxygen vacancy complex with hydrogen is globally a negative-*U* center.

In the positive charge state, the energy difference between the global minimum, $[SiH+O(3)^{+}]$, and the positive hydrogen bridge $[SiH(2)Si^{+}]$ is only 0.05 eV, which is comparable to thermal energies and not very significant. However, in the negative charge state $[SiH+SiSi(5)^{-}]$ is 0.62 eV more stable than $[SiH(2)Si^{-}]$. In the paramagnetic neutral charge state the situation is reversed and [SiH(2)Si] is more stable than neutral [SiH+Si(3)] by 0.16 eV. Including the correction for the compensating background, we find the two metastable partners isoenergetic within 0.1 eV for Fermi levels below the position of the Si conduction band, and the $[SiH+SiSi(5)^{-}]$ more stable up to 0.64 eV for Fermi levels lying higher than it.

The activation energy given in Table V between the two metastable complexes increases with the number of electrons from 0.3 eV in the positive charge state to 0.9 eV in the neutral charge state. The correlation between activation energies and charge state is naturally explained by the promotion energy of electrons from an sp^3 orbital to a higher-lying *p* orbital in the planar transition state. The transition state for the negative charge state has not been calculated, because the *p* orbital enters into the DFT conduction band, resulting in a qualitatively incorrect description of the electronic structure due to the underestimated Kohn-Sham conduction band edge. However, following the argument given above, a barrier of 1–2 eV can be anticipated. This finding has implications on diffusion mechanisms involving undercoordinated silicon atoms. An empty dangling bond will easily reverse its direction, whereas an occupied dangling bond will face a large barrier.

The barrier between the hydrogen bridge and the [SiH +Si(3)] defect has been calculated by Rudra, Fowler, and

TABLE XVII. Structural parameters of the transition state for the conversion of the positive hydrogen bridge $[SiH(2)Si^{+}]$ into $[SiH+O(3)^{+}]$. O(3) refers to the oxygen atom that is threefold-coordinated in the defect $[SiH+Si(3)^{+}]$. The distances to the generic atom O are obtained as the average value over the three nearest-neighbor distances to the corresponding silicon atom.

	$[SiH(2)+Si]$ $\updownarrow$ $[SiH+O(3)^{+}]$	$[SiH(2)Si]$ $\updownarrow$ [SiH+Si(3)]
$d(Si_{(1)}\text{-}H)$	A1.496 Å	1.498 Å
$d(Si_{(2)}\text{-}H)$	2.503 Å	2.256 Å
$d(Si_{(1)}\text{-}Si_{(2)})$	3.836 Å	3.581 Å
∠[Si(1)-H-Si(2)]	146.0°	144.2°
$t(Si_{(1)})$	0.956	0.962
$t(Si_{(2)})$	0.060	0.003
$d[Si_{(2)}\text{-}O(3)]$	2.567 Å	3.076 Å
$d(Si_{(1)}\text{-}O)$	1.627 Å	1.628 Å
$d(Si_{(2)}\text{-}O)$	1.574 Å	1.642 Å

TABLE XVIII. Structural parameters for the hydrogen bridge [SiH(2)Si] in the three charge states.

	$[SiH(2)^+Si]$	[SiH(2)Si]	$[SiH(2)^-Si]$
$d(Si_{(1)}\text{-}H)$	1.646Å	1.534Å	1.450Å
$d(Si_{(2)}\text{-}H)$	1.710Å	1.953Å	2.220Å
$d(Si_{(1)}\text{-}Si_{(2)})$	3.225Å	3.368Å	3.441Å
∠[Si(1)-H-Si(2)])	147.8°	149.7°	138.4°
$t(Si_{(1)})$	0.565	0.892	0.984
$t(Si_{(2)})$	0.403	1.025	1.848
$d[Si_{(2)}\text{-}O(3)]$	3.439Å	3.410Å	3.509Å
$d(Si_{(1)}\text{-}O)$	1.597Å	1.631Å	1.644Å
$d(Si_{(2)}\text{-}O)$	1.591Å	1.644Å	1.739Å

Feigl using the semiempirical electronic structure methods to be 0.6 eV, i.e., 0.3 eV lower than our barrier.[86] The relative stability is reversed. Whereas I find the neutral hydrogen bridge to be more stable by 0.16 eV, Rudra, Fowler, and Feigl find the [SiH+Si(3)] defect more stable by 0.1 eV. The difference lies within the uncertainty of semiempirical methods.

Interesting is that positive charging of the neutral [SiH +Si(3)] defect generates hydrogen bridges. This finding resulted from a dynamical simulation from the relaxed structure of the [SiH+Si(3)] defect after removal of an electron. This result is confirmed by the longer distance between silicon and oxygen denoted $d(Si_{(2)}\text{-}O(3))$ in Table XVI in the ground state of the neutral [SiH+Si(3)] defect compared to the distance in the transition state for the interconversion of $[SiH(2)Si^+]$ and $[SiH+O(3)^+]$ given in Table XVII.

Owing to the large energy barrier between the two metastable configurations in the negative charge state, the interconversion is expected to occur only in the positive and neutral charge states. In those charge states, both configurations have similar energies. At room temperature I expect an interconversion every 10–100 sec. In the positive charge state, interconversions occur on the submicrosecond time scale, whereas in the negative charge state an interconversion will occur every few thousand years. Hence I expect the two configurations two occur in similar concentrations in a tunneling experiment even though the ''effective'' Fermi level of this nonequilibrium situation lies in the energy region where the $[SiH+SiSi(5)^-]$ is thermodynamically favored.

The complex formation between an oxygen vacancy and atomic hydrogen is exothermic

$$[SiSi]+[O(3)^+H]\rightarrow[SiH+O(3)^+] \quad \Delta E=-0.7 \text{ eV}$$

in the positive and

$$[SiSi]+[Si(5)^-H]\rightarrow[SiH+SiSi(5)^-] \quad \Delta E=-0.5 \text{ eV}$$

in the negative charge state, using the values from Table VII. (In the neutral charge state the reaction energy is even higher, i.e., 1.5 eV.) Thus we can assume that oxygen vacancies will be decorated with hydrogen in the presence of atomic hydrogen. However, the binding energy is sufficiently small that hydrogen removal from the oxygen vacancy is possible by a high-temperature anneal.

A. Positive hydrogen bridge: $[SiH(2)Si^+]$

The positive hydrogen bridge is not straight, but has a bond angle of 148°, and is 5% longer than an oxygen bridge, see Table XVIII. Both SiH bonds (1.65 and 1.71 Å) are about 10–15% longer than an isolated [SiH] fragment. The hydrogen position is slightly asymmetric with one SiH bond 4% longer than the other.

B. Neutral hydrogen bridge [SiH(2)Si] and E_4'

The hydrogen position of the neutral hydrogen bridge is more asymmetric than in the positive charge state, see Table XVIII. Two different configurations have been found with the hydrogen atom localized more on one or the other silicon atom. I found both structures to be isoenergetic (within 4 meV).

When the defect traps an electron the main relaxation is a further bending of the hydrogen away from the lone pair at the silicon. The structural relaxation energy of 0.87 eV is small compared to other defect relaxations of charge-state changes in silica. The relaxation is driven by a downshift of the charge-state level by 1.70 eV.

Hyperfine parameters

The E_4' center[32,40,49,89] has been attributed to a neutral charge state of the hydrogen bridge.[32]

The spin density corresponds to the SiSi antibond, which can also be viewed as a silicon dangling bond on one silicon atom with an antibonding interaction with the SiH bond orbital. The hydrogen atom has only small hyperfine parameters because it is located near the node plane of the orbital.

The isotropic hyperfine parameter is found to be 42 mT on the long-bond side and 18.5 mT on the short-bond silicon, see Table XIX. The hydrogen hyperfine parameter is only 1.2–1.4 mT, which is due to the location near the node plane of the orbital giving rise to the spin density. Experimentally the hyperfine parameters of the E_4' center vary substantially with temperature. At low temperature the measured silicon Fermi-contact terms are 44.5 and 7.7 mT, which shift towards each other by 8 mT each at 300 K. The temperature variation results from transitions between the two metastable configurations of the neutral hydrogen bridge.[32]

There are important deviations from experiment that cannot be attributed to errors of methodology, and hence must

TABLE XIX. Hyperfine parameters (A in mT) and directions (θ,φ in degrees) of the E_4' center. Only two silicon neighbors of Si(1) have appreciable hyperfine parameters.

	This work		This work		Expt. (Ref. 32)	
	A	(θ,φ)	A	(θ,φ)	A	(θ,φ)
H(1)	1.2	(55,64)	1.4	(55,73)	2.1	(54,78)
	−2.3	⊥	−2.1	⊥	0.3	(106,0.0)
	−2.3	⊥	−2.1	⊥	0.2	(41,290)
Si(1)	−20.0	(110,229)	−47.4	(108,225)	−8.5	(104,216)
	−17.7	⊥	−42.4	⊥	−7.3	(94,307)
	−17.7	⊥	−42.4	⊥	−7.3	(166,54)
Si(2)	−45.3	(42,98)	−19.1	(39,92)	−48.7	(43,84)
	−40.3	⊥	−16.8	(100,169)	−42.5	(97,167)
	−40.3	⊥	−16.7	(52,251)	−42.5	(47,251)
Si(1a)	−0.6	(30,100)	−1.3	(26,127)		
	−0.5	⊥	−1.1	⊥		
	−0.5	⊥	−1.1	⊥		
Si(1b)	−0.3	(59,259)	−1.0	(61,268)		
	−0.2	⊥	−0.9	⊥		
	−0.2	⊥	−0.9	⊥		
Si(2a)	−0.3	(71,177)	−0.1	(72,185)		
	−0.2	(19,2)	0.0	⊥		
	−0.1	(92,87)	0.0	⊥		
Si(2b)	−0.6	(122.5,59)	−0.2	(123,57)		
	−0.5	⊥	−0.1	⊥		
	−0.5	⊥	−0.1	⊥		
Si(2c)	0.1	⊥	0.1	(60,338)		
	0.1	⊥	0.0	⊥		
	0.1	⊥	0.0	⊥		

be attributed either to quantum-mechanical effects of the proton or to a deficiency of the density functionals used. Our calculations predict a smaller asymmetry between the two silicon hyperfine parameters than that observed in low-temperature experiments. Second, the sum of hyperfine splittings, which is nearly temperature independent, is overestimated by 8 mT, i.e., 5%, in our calculations. This finding implies that the spin density is too delocalized in our calculations. The most likely explanation is that the length of the hydrogen bridge is underestimated. A larger Si–Si distance would result in a further localization of the hydrogen on one and a localization of the spin density on the other silicon atom. This underestimate may be an artifact of the density functionals used. However, quantum effects of the proton cannot be ruled out. The quantum-mechanical delocalization of the proton may weaken the hydrogen bridge. On the other hand, the delocalization may also result in more symmetric hyperfine parameters because of quantum-mechanical tunneling between the two sites. Therefore the hydrogen bridge presents itself as an interesting test case for new density functionals.

C. Negative hydrogen bridge [SiH(2)Si$^-$]

The hydrogen position becomes even further asymmetric in the negative charge state, see Table XVIII. Now the short SiH bond is comparable in distance to an unperturbed SiH bond as found in [SiH+O(3)$^+$], [SiH+Si(3)], and [SiH +SiSi(5)]. The tetrahedral distortion on the other silicon atom grows to a value close to 2, which is typical for lone pairs on undercoordinated silicon atoms, as seen also in the [Si(3)$^-$+O(3)$^+$] ion-pair oxygen vacancy.

D. Positive [SiH+O(3)$^+$]

The positive hydrogen bridge is only a metastable state of the hydrogenated oxygen vacancy. A transformation analogous to that from the E_δ' to the E_γ' center results in the precursor of the E_β' center, which is called E_2' in α quartz. This defect can be considered a pair of silane-group [SiH] and a positively charged, threefold-coordinated oxygen center [O(3)]. It exhibits only shallow levels close to the band edges of silica and may be a fixed or slow positive charge defect.

The stable configuration of the hydrogenated positive oxygen vacancy, $[\mathrm{SiH}+\mathrm{O(3)}^+]$, corresponds structurally and electronically to the metastable configuration of the neutral oxygen vacancy $[\mathrm{Si(3)}^- + \mathrm{O(3)}^+]$. The additional proton stabilizes the lone pair of the oxygen vacancy and avoids the unstable ion-pair configuration. This defect can be considered a nearly independent pair consisting of an overcoordinated oxygen an a SiH bond. It is likely that the overcoordinated oxygen atom is able to diffuse away and thus provide a precursor of an isolated dangling-bond defect E_s'.

E. Neutral [SiH+Si(3)] and E_2' or E_β'

The neutral $[\mathrm{SiH}+\mathrm{Si(3)}]$ defect exhibits a silicon dangling bond that does not interact with other sites of the lattice. The reduced binding results in reduced stability compared to the hydrogen bridge [SiH(2)Si], the latter now being 0.15 eV lower in energy.

The $[\mathrm{SiH}+\mathrm{Si(3)}]$ defect has been attributed to the E_2' center.[86] Weeks and Nelson[40,49] characterized this defect by bleaching its ESR signal with light, temperature, and an optical absorption line of 5.39 eV. This line agrees perfectly with the position of the 0/+ switching charge-state level of $[\mathrm{SiH}+\mathrm{Si(3)}]$: Exciting an electron from this level to the conduction band requires 5.36 eV, in perfect agreement with experiment. The excitation from the valence band into the defect level would require 6.56 eV. Given the uncertainties of determining the band edges relative to the defect levels, the assignment of this adsorption should, however, be taken with a grain of salt.

In order for this assignment of the optical absorption line to be valid, the position of the +/++ level of E_1' or $[\mathrm{Si(3)}+\mathrm{O(3)}^+]$ relative to the conduction band should match the absorption line of 5.9 eV observed by Nelson and Weeks[40,49] for the E_1' center. I have not done that calculation, but estimate it from the +/0 switching level and the Coulomb repulsion U of the $[\mathrm{SiH}+\mathrm{Si(3)}]$ defect as example of an s silicon-dangling-bond center. The Coulomb repulsion for the $[\mathrm{SiH}+\mathrm{Si(3)}]$ is $U=\epsilon_{\mathrm{sw}}(0/-)-\epsilon_{\mathrm{sw}}(0/+)=2.48$ eV. (This positive U value for a fixed structure does not contradict the negative-U property of the defect, which also considers structural relaxations.) The +/0 switching level of the $[\mathrm{Si(3)}+\mathrm{O(3)}^+]$ defect lies 0.68 eV above the reference energy and 3.45 eV below the (non-DFT) conduction band. By adding the Coulomb repulsion we obtain 5.93 eV in perfect agreement with experiment. The difference of 0.5 eV between the absorption lines of E_2' and E_1' can be attributed to the difference in electrostatic potentials of the positive overcoordinated oxygen on the one hand and the neutral SiH fragment on the other. Pacchioni and Ierano recently calculated the optical transitions using accurate multireference configuration interaction (CI) calculations on clusters.[47] As suggested by Griscom and Fowler,[90] they identified the absorption band of the E_1' center with a charge-transfer transition from the silicon dangling bond to the silicon atom bound to the overcoordinated oxygen atom,[47] and obtained an absorption energy of 5.8 eV.

Given that the conduction band is built up of silicon levels, the charge-transfer transition in the cluster is most likely the same process as the excitation to the conduction band or a shallow donor state. The main difference between the two pictures is the extent of the localization of the final one-electron state. The localization of the final state will be determined by a tradeoff between the Coulomb attraction of the conduction electron to the positive $[\mathrm{O(3)}^+ + \mathrm{Si(3)}^+]$ and the kinetic energy required to localize the wave packet. The close correlation of the calculated Coulomb repulsion in a silicon dangling bond and the measured difference in absorption energies of the E_2' and E_1' centers indicate that the final state for the electron does not have a large Coulomb repulsion, which is indicative of a delocalized state.

Let us estimate the energies and the extent of the wave functions of the donor levels in an effective-mass picture. Note that in this case the theory discussed below is stretched beyond the limits of its applicability and that its conclusions are to be taken only as qualitative guidelines. The emerging physical picture may nevertheless be instructive. The degree of localization of a ''shallow'' donor state is estimated using the effective mass of $m^*=0.6m_0$ for electrons at the oxide conduction band.[91,92] The dielectric constant of silica is $\epsilon_r = 4.48\,\epsilon_0$.[14] Within the effective-mass approximation, the donor level is expected at $E=(m^*Z^2e^4/(2\epsilon_r^2\hbar^2)$ below the conduction band edge, and has a classical radius of $r_0 = \hbar^2\epsilon_r/(Ze^2m^*)$.

For the E_2'/E_β' center we use $Z=1$, which yields a state 0.44 eV below the conduction-band edge and a radius of 3.95 Å . In this case the effective-mass approximation may be marginally applicable, because the wave function extends over several sites. A correction to our estimate for the transition energy of order 0.44 eV must be considered.

As the radius of the donor orbital is smaller than the distance between the two silicon atoms, I describe the double positive defect as being two $Z=1$ centers with one electron that interact electrostatically. This is analogous to a H_2^+ molecule, which, however, is strongly asymmetric because of the different structural environments of the two centers. In the bond state the electron would be localized on the donating silicon atom, whereas the antibonding state would be localized on the electron-accepting silicon atom. In orbital terminology it may be described as an sp^3 hybrid pointing towards the dangling bond. It is therefore not surprising that the charge-transfer transition which occupies this orbital reforms the SiSi bond of the E_3' center. The transition from the bonding to the antibonding state in the effective-mass picture is therefore exactly a charge transfer transition. For the E_1' center the description of a charge-transfer transition is clearly appropriate, whereas the transition of the E_2' center can be reasonably described as an excitation of an electron into the conduction band.

A still unexplained fact is that the absorption band attributed to the E_1' and E_2' centers can be reversibly interconverted by optical bleaching experiments.[40] One may speculate that the coupling of the two defects occurs via electron exchange through the conduction band. This process would imply the existence of doubly positive oxygen vacancies, probably in the form of a pair of $[\mathrm{O(3)}^+]$ defects in close proximity to each other, and singly positive hydrogen complexes with an oxygen vacancy such as $[\mathrm{SiH}+\mathrm{O(3)}^+]$ after γ irradiation. These defects could capture electrons through their shallow donor levels, and develop into E_1' and E_2' centers.

TABLE XX. Hyperfine parameters (A in mT) and directions (θ,φ in degrees) of the E_2' center. Only atoms with hyperfine parameters exceeding 0.1 mT are shown.

	A	(θ,φ)		A	(θ,φ)
H(1)	0.2	(47,79)	Si(1)	48.9	(45.6,89)
	0.0	$\perp$		43.2	$\perp$
	0.0	$\perp$		43.2	$\perp$

Hyperfine parameters

I obtain a Fermi contact term on silicon of 45.1 mT, which is in the range of other silicon dangling bonds, see Table XX. The spin density is clearly localized on only one silicon dangling bond, resulting in a very small hyperfine parameter on hydrogen, and no hyperfine parameters larger than 0.2 mT on other silicon atoms.

Hyperfine parameters have been measured by Weeks.[85] Unfortunately the hyperfine parameters of the E_2' center have not been analyzed in the same detail as the E_1' and E_4' centers.

Weeks[85] (see also Ref. 93) measured an axial hyperfine parameter on the hydrogen of 0.14 mT and an equatorial hyperfine parameter of -0.02 mT, where axial refers to the direction parallel to the axis of the g tensor. The deviation of our result from Weeks' data is in the range expected from our methodology. The predictions for the isotropic part on the silicon are 43 mT, which is 2 mT or 4% lower than our calculations. The calculated anisotropy of 5.7 mT is in good agreement with the measured value of 5.4 mT.

F. Negative hydrogenated oxygen vacancy $[\mathrm{SiH+SiSi(5)^-}]$

Interestingly I find that the lone pair in the negative hydrogenated oxygen vacancy forms a bond to a silicon atom, which becomes fivefold-coordinated in a trigonal bipyramidal structure. To our knowledge, this is the first proposal for such a structure. The bonding description of the fivefold-coordinated silicon in this defect is analogous to that of the negative hydrogen: Three bonds involving sp^2 orbitals of the silicon and a three-center bond (see Fig. 6) in the axial direction, with a doubly occupied nonbonding orbital. The SiSi bond is 7% longer than the bond the neutral oxygen vacancy [SiSi], which is attributed in part to the axial bond elongation and in part to bond strain.

VII. COMPLEX OF TWO HYDROGEN ATOMS WITH AN OXYGEN VACANCY

Complexes of hydrogen molecules with oxygen vacancies are of particular interest for Bragg gratings,[94] and as an intermediate for the interconversion of hydrogen molecules into atomic hydrogen.[95] Bragg gratings invented by Hill *et al.*[96] are periodic variations of the refractive index of optical fibers on a micrometer length scale, which are used to reflect light of a well-defined wavelength. Bragg gratings exploit the photosensitivity of doped silica towards UV irradiation.[94] Large index variations have been obtained after prior loading of the fiber with hydrogen.[97]

As discussed above, hydrogen molecules do not react with the unperturbed framework. In the presence of an oxygen vacancy, however, the hydrogen complex is thermodynamically stable against dissociation, and can form a pair of two SiH groups.

TABLE XXI. Structural parameters of the oxygen vacancy complex with two hydrogen atoms, $[(\mathrm{SiH})_2]$ and its positive charge state.

	$[(\mathrm{SiH})_2^+]$	$[(\mathrm{SiH})_2]$
$d(\mathrm{Si_{(1)}\text{-}H_{(1)}})$	1.600 Å	1.453 Å
$d(\mathrm{Si_{(2)}\text{-}H_{(2)}})$	1.622 Å	1.462 Å
$d(\mathrm{H_{(1)}\text{-}H_{(2)}})$	1.002 Å	1.811 Å
$d(\mathrm{Si_{(1)}\text{-}Si_{(2)}})$	3.879 Å	3.574 Å

The stability of the pair of two SiH groups is an indication that the oxygen vacancy is not only unstable with respect to complex formation with a single atomic hydrogen, but that the hydrogen complexes react further with an atomic hydrogen that forms SiH fragments.

$$[\mathrm{SiH+SiSi(5)^-}]+[\mathrm{O(3)^+H}]\rightarrow[(\mathrm{SiH})_2]$$

$$\Delta E=-3.05\ \mathrm{eV},$$

$$[\mathrm{SiH+O(3)^+}]+[\mathrm{Si(5)^-H}]\rightarrow[(\mathrm{SiH})_2]\quad \Delta E=-2.84\ \mathrm{eV}.$$

This is an indication that there is a large reservoir of bound hydrogen in the silica that is not active electrically. Hot electrons with an energy of approximately 3 eV may dissociate atomic hydrogen from these silane groups and create electrically active hydrogen complexes with an oxygen vacancy from SiH groups under formation of molecular hydrogen, such as the hydrogen bridge. This picture is in general agreement with the hydrogen model of Griscom[2] and DiMaria, Cartier, and Arnold.[3] However, one should note that hydroxyl groups have yet to be taken into account. Hydroxyl groups are expected to be even more stable than SiH groups.

A. Complex of two hydrogen atoms with an oxygen vacancy: $[(\mathrm{SiH})_2]$

An oxygen vacancy forms two silane groups, see Table XXI and Fig. 10. In the neutral charge state the SiH bonds are comparable in bond length to that of the hydrogenated oxygen vacancy [SiH+Si(3)].

The charge-state level for positive charging is located 3.67 eV below the reference energy. This orbital can be considered an antibonding state between the two hydrogen atoms, or the two SiH-bond orbitals.

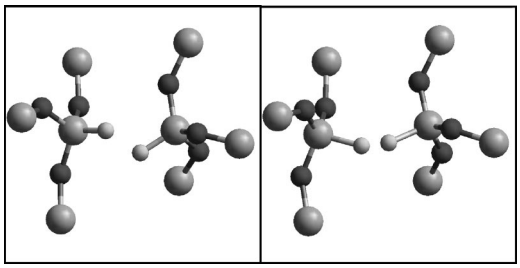

FIG. 10. Structure of the oxygen vacancy interacting with two hydrogen atoms $[(\mathrm{SiH})_2]$ in the neutral (left) and positive (right) charge states.

B. Complex of two hydrogen atoms with a positive oxygen vacancy: $[(SiH)_2^+]$

The pair of two silane groups has an orbital in the lower region of the band gap. By removing one electron from the antibonding orbital of the two hydrogen atoms, the antibond is weakened considerably, causing the close approach of the two hydrogen atoms. The distance between the hydrogen atoms is now only 35% larger than in the hydrogen molecule, see Table XXI. The charging of the doubly hydrogenated oxygen vacancy is sufficient to bring the defect energetically within the energy of a pair of [SiH(2)Si] and $[O(3)^+]$, which is likely to provide a pathway for the dissociation of hydrogen molecules.

VIII. CONCLUSION

A comprehensive study of defects related to oxygen vacancies and hydrogen in quartz has been presented. Hydroxyl groups and isolated silane fragments have been excluded from the present study, because the latter two defects are fairly stable and relatively inert. We investigated structure, energetics, charge states, and hyperfine parameters.

Most defects studied can be composed of a small number of structural motifs such as overcoordinated oxygen atoms, overcoordinated silicon atoms, as well as undercoordinated silicon atoms. Silicon dangling bonds [Si(3)] occupied by one electron are responsible for a suite of E' centers. They exhibit a localized spin that gives rise to characteristic ESR signals. In the positive charge state, dangling bonds have a tendency to attack an oxygen bridge and form threefold-coordinated oxygen atoms $[O(3)^+]$. Overcoordinated oxygen atoms are the classical positive charge defects in silica. This defect does not introduce levels in the band gap, except a shallow donor orbital below the conduction-band edge. The absence of deep levels in the gap may cause the slow charging behavior of $[O(3)^+]$-related defects. Doubly occupied silicon dangling bonds have a tendency to attack silicon atoms, thus forming a defect $[SiSi(5)^-]$. Overcoordinated silicon atoms $[Si(5)^-]$ can be considered the classical negative charge defect in silicon. Hydrogen behaves behaves qualitatively similar to silicon dangling bonds: it binds to an oxygen bridge in the positive charge state, it binds to a silicon atom in the negative charge state, and it does not bind to the lattice at all in the neutral state.

With a few exceptions, all defects exhibit a tendency to rebond under electron and hole capture. The large structural relaxations under charge-state changes result in high relaxation energies of the charge-state levels and charge trapping at the defect. This causes many of the defects to be negative-U defects: they are thermodynamically unstable in the paramagnetic charge state. This is considered the underlying cause of the general tendency of silicon to oxide charging and the large level shifts of switching charge-state levels. In particular I found that the E_1' center, the counterpart of the E_γ' center in quartz, is too high in energy (~ 3 eV) to be formed under normal device operations of MOSFET's.

Only the hydrogen bridge exhibits small relaxations of the switching charge-state levels,[6] which is a precondition for carrying a tunnel current in a two-step tunneling process, which requires the energy dissipation of the electron at the defect to be smaller than the applied voltage. The shift of the $0/-$ switching level upon charging is 1.7 eV and that of the $+/0$ level is 2.1 eV. At higher voltages of 3 eV relevant for experiment, the $0/-$ transition of the [SiH+Si(3)] can also contribute to tunneling.

All defects involving a single hydrogen have a thermodynamic charge state within or near the silicon band gap. Therefore both positive and negative charge states of these defects are accessible with a low voltage applied across a MOS structure. I have attributed the $+/-$ thermodynamic charge-state level to the interface state observed 0.2 eV above the silicon midgap energy in *C-V* experiments.[6]

Both the oxygen vacancy and the hydrogenated oxygen vacancy exhibit metastable states. The barrier for the transition between the metastable states increases with the number of electrons on the defect, because the transition state is destabilized by electrons in the high-lying p state perpendicular to the plane spanned by the three remaining oxygen neighbors.

The tendency of silicon to fivefold coordination may suggest new diffusion mechanisms for oxygen surplus centers, such as undercoordinated oxygen atoms, which may easily interconvert to a defect with fivefold-coordinated silicon atoms. Work to investigate such diffusion mechanisms is in progress.

The oxygen vacancy concentration obtained from the equilibrium with the position of the Si/Si_2 interface is in agreement with the measured vacancy concentrations near the interface. In this process, oxygen vacancies can be introduced into the oxide by oxidizing silicon, which in effect shifts the phase boundary. Previous assumptions[98] were based on an equilibrium of the oxygen vacancy concentration between oxygen interstitials in the silicon, assuming a rigid phase boundary. This tied the vacancy concentration to the oxygen contribution of silicon. Near the interface, however, oxygen interstitials in silicon and oxygen vacancies in the oxide both are in equilibrium with the interface, and are determined by the oxidization process, not by the bulk silicon. Because the formation energies of oxygen vacancies in silica and of oxygen interstitials[98] in silicon are similar, the two models may be hard to distinguish experimentally. This equilibrium also suggests that the production of oxygen vacancies at the interface is one contributing mechanism of silicon oxidation.

Calculated hyperfine parameters are in unprecedented good agreement with experiments. Thus the previous assignments of the ESR spectra to structural models of the defects have been confirmed. Furthermore, these calculations establish the accuracy of the PAW method for calculations of hyperfine parameters.

ACKNOWLEDGMENTS

It is a pleasure to thank J. H. Stathis and T. Theiss for pointing out the relevance of hydrogen chemistry in gate oxides, and for invaluable discussions and suggestions on the topic. I am also indebted to J. G. Bednorz, G. L. Bona, E. Cartier, R. Germann, E. Gousev, S.T. Pantelides, W. Rieß, H. W. M. Salemink, Y. Tu, and C. G. Van de Walle for discussions and useful hints throughout the project.

APPENDIX: HYPERFINE PARAMETERS

The scalar relativistic expression[30] of the Fermi-contact term differs from the nonrelativistic expression in that the δ function in the nonrelativistic expression Eq. (2) is replaced by a more extended function,

$$\delta_T(r)=\frac{1}{4\pi r^2}\partial_r\frac{m_e}{M}\approx\frac{1}{4\pi r^2}\frac{2}{r_T}\frac{1}{(1+2r/r_T)^2}, \quad \text{(A1)}$$

which is localized within the Thomson radius $r_T=Ze^2/(4\pi\epsilon_0 m_e c^2)$. $M(r)=m_e+[\epsilon-V(r)]/(2c^2)$ is the relativistic mass, obtained from the potential $V(r)$ and the one-particle energy ϵ. The approximate form is obtained by replacing $\epsilon-V$ by $Ze^2/(4\pi\epsilon_0 r)$.

When evaluating the anisotropic hyperfine interaction term, we use

$$\partial_i\partial_j\frac{1}{|r|}=-\frac{4\pi}{3}\delta_{i,j}\delta(r)+\frac{1}{|r|^3}\frac{3r_ir_j-\delta_{i,j}r^2}{r^2}, \quad \text{(A2)}$$

which allows the integral for the anisotropic hyperfine parameter to be rewritten as

$$\int d^3r\frac{n_s(r)}{r^3}\frac{3r_ir_j-\delta_{i,j}r^2}{r^2}=\left(\partial_i\partial_j-\frac{1}{3}\delta_{i,j}\nabla^2\right)\int d^3r'\frac{n_s(r')}{|r-r'|}. \quad \text{(A3)}$$

This equation shows the equivalence of the electrostatic or magnetostatic interaction between two dipoles on the one side and a monopole and a quadrupole on the other side. The expression for the magnetic hyperfine parameters is therefore analogous to those for the isomer shift and the electric-field gradient. The main difference is that the magnetic hyperfine parameter is obtained from the spin density, while the isomer shift and the electric field gradients are obtained from the total density.

Let us introduce here the auxiliary variables

$$w(r)=\int dr\frac{n_s(r')}{|r-r'|} \quad \text{(A4)}$$

and

$$W_{i,j}(R)=\left(\partial_i\partial_j-\frac{1}{3}\delta_{i,j}\nabla^2\right)|_R w(r),$$

which allows us to express the hyperfine interaction as

$$A_{i,j}=\frac{g^e\mu^e}{\hbar}\gamma_N\left[\frac{2\mu_0}{3}\delta_{i,j}\int d^3r\,\delta_T(r-R)n_s(r)+\frac{\mu_0}{4\pi}W_{i,j}(R)\right], \quad \text{(A5)}$$

where R is a nuclear position.

In the PAW method, the spin density $n_s(r)=\tilde{n}_s+n_s^1-\tilde{n}_s^1$ is a superposition of the pseudospin density $\tilde{n}_s(r)$ and the difference between the one-center expansions of the true spin density, $n^1(r)$, and those of the pseudo-spin density, $\tilde{n}_s^1(r)$. Similarly, we obtain $w(r)=\tilde{w}(r)+w^1(r)-\tilde{w}^1(r)$ and $W_{i,j}=\tilde{W}_{i,j}+W^1_{i,j}-\tilde{W}^1_{i,j}$ from the corresponding pseudo- and one-center contributions. The pseudospin density is obtained from the pseudowave functions, i.e. the plane parts of the wave functions. The one-center expansions are obtained as products of partial waves on radial, atom-centered logarithmic grids multiplied with real spherical harmonics. Relativistic expressions are applied only to the all-electron quantities, whereas nonrelativistic expressions are consistently used for the pseudowave functions and their one-center expansions.

From the plane wave expansion of the pseudodensity we obtain

$$\tilde{n}_s(R)=\sum_G\tilde{n}_s(G)e^{iGR},$$

needed for the contact interaction, and

$$\tilde{W}_{i,j}=\sum_G\frac{-4\pi\langle G_iG_j-\frac{1}{3}G^2\rangle}{G^2}\tilde{n}_s(G)e^{iGR},$$

required for the anisotropic parameters.[99]

Some care is needed during the integration because the relativistic s-wave functions diverge near the nucleus as $\Psi_s\approx r^{\sqrt{1-\alpha^2Z^2}-1}$ and because the function δ_T cannot be considered smooth relative to the grid spacing of the radial logarithmic grid.

For the integration from the origin to the first grid point, we represent the density as $n_s(r)=(r/r_1)^{\sqrt{1-\alpha^2Z^2}-1}\Sigma_i c_i r^i$, where the polynomial is of third order and the coefficients are obtained by matching the density of the four innermost radial grid points. The integral to the second grid point is performed using a Taylor expansion of $\delta_T(r)$ about r_2,

$$\int_{r<r_2}d^3r\,\delta_T(r)\rho(r)=\sum_{i,j=0}\frac{c_ix^{q+i}(j+1)}{(q+i)(1+x)^2}\times\prod_{k=1}^{j}\left[\frac{1}{1+\frac{q+i}{k}\left(\frac{x}{1+x}\right)}\right], \quad \text{(A6)}$$

where $x=2r_2/r_T$ and $q=2(\lambda-1)+1$. Note that a Taylor expansion about the origin has a convergence radius of only $r_T/2$ because of the pole at $|r|=-r_T/2$, so that the resulting expression would diverge for $2r_2>r_T$. The expression provided here converges within 100 iterations for $Z\geq 1$.

In between the radial grid points, beginning with the interval from the second to the third grid point, the spin density is represented for each interval of consecutive grid points by a third-order interpolating polynomial. The resulting integrals can be evaluated analytically.

For the anisotropic hyperfine parameters, we determine $w(r)$ on the radial grid by solving the radial Poisson equation for the spin density n_s^1. The matrix $W_{i,j}$ is then obtained from the $l=2$ contribution of $w(r)=\Sigma_{l,m}w_{l,m}(|r-R|)Y_{l,m}(r-R)$ as

$$W^1_{i,j}=\sum_{m,l=2}\left(\lim_{r\to R}\frac{w^1_{l,m}}{|r-R|^2}\right)\left[\partial_i\partial_j-\frac{1}{3}\delta_{i,j}\nabla^2\right]\times(r-R)^2Y_{l,m}(r-R), \tag{A7}$$

which results in

$$W^1_{xx}=2\sqrt{\frac{15}{16\pi}}\lim_{r-R}\frac{w^1_{x^2-y^2}}{|r-R|^2}-2\sqrt{\frac{5}{16\pi}}\lim_{r-R}\frac{w^1_{3z^2-r^2}}{|r-R|^2},$$

$$W^1_{yy}=-2\sqrt{\frac{15}{16\pi}}\lim_{r-R}\frac{w^1_{x^2-y^2}}{|r-R|^2}-2\sqrt{\frac{5}{16\pi}}\lim_{r-R}\frac{w^1_{3z^2-r^2}}{|r-R|^2},$$

$$W^1_{zz}=6\sqrt{\frac{5}{16\pi}}\lim_{r-R}\frac{w^1_{3z^2-r^2}}{|r-R|^2},$$

$$W^1_{xy}=W^1_{xy}=\sqrt{\frac{60}{16\pi}}\lim_{r-R}\frac{w^1_{xy}}{|r-R|^2},$$

$$W^1_{xz}=W^1_{zx}=\sqrt{\frac{60}{16\pi}}\lim_{r-R}\frac{w^1_{xz}}{|r-R|^2},$$

$$W^1_{yz}=W^1_{zy}=\sqrt{\frac{60}{16\pi}}\lim_{r-R}\frac{w^1_{yz}}{|r-R|^2},$$

using the special form of the real spherical harmonics.

[1] D. J. DiMaria and J. Stathis (unpublished).
[2] D. L. Griscom, J. Electron. Mater. **21**, 762 (1992).
[3] D. J. DiMaria, E. Cartier, and D. Arnold, J. Appl. Phys. **73**, 3367 (1993).
[4] D. J. DiMaria and E. Cartier, J. Appl. Phys. **78**, 3883 (1995).
[5] J. H. Stathis, Appl. Phys. Lett. **68**, 1669 (1996).
[6] P. E. Blöchl and J. Stathis, Phys. Rev. Lett. **83**, 372 (1999).
[7] P. Hohenberg and W. Kohn, Phys. Rev. **136**, B864 (1964); W. Kohn and L. J. Sham, Phys. Rev. **140**, A1133 (1965).
[8] J. P. Perdew and Y. Wang, Phys. Rev. B **45**, 13 244 (1992).
[9] J. P. Perdew, K. Burke, and M. Ernzerhof, Phys. Rev. Lett. **77**, 3865 (1996).
[10] P. E. Blöchl, Phys. Rev. B **50**, 17 953 (1994).
[11] The hyperfine parameters of hydrogen have been extracted with $E_{\mathrm{PW}}=70$ Ry.
[12] J. Glinnemann, H. E. King, Jr., H. Schulz, T. Hahn, S. J. La Place, and F. Dacol, Z. Kristallogr. **198**, 177 (1992).
[13] L. Levien, C. T. Prewitt, and D. J. Weidner, Am. Mineral. **65**, 920 (1980).
[14] K. F. Young and H. P. R. Frederikse, J. Phys. Chem. Ref. Data **2**, 313 (1973).
[15] D. R. Hamann, Phys. Rev. Lett. **76**, 660 (1996).
[16] *CRC Handbook of Chemistry and Physics*, 64th ed. (CRC, Boca Raton, 1983).
[17] F. Liu, S. Garofalini, D. King-Smith, and D. Vanderbilt, Phys. Rev. B **49**, 12 528 (1994).
[18] Z. A. Weinberg, G. W. Rubloff, and E. Bassous, Phys. Rev. B **19**, 3107 (1979).
[19] H. R. Phillipp, Solid State Commun. **4**, 73 (1966).
[20] T. H. DiStefano and D. E. Eastman, Solid State Commun. **9**, 2259 (1970).
[21] N. F. Mott, J. Non-Cryst. Solids **40**, 1 (1980).
[22] S. Miyazaki, H. Nishimura, M. Fukuda, L. Ley, and J. Ristein, Appl. Surf. Sci. **113/114**, 585 (1997).
[23] H. Balamane, T. Halicioglu, and W. A. Tiller, Phys. Rev. B **46**, 2250 (1992).
[24] Calculations done in a 64-silicon-atom unit cell with Γ-point sampling only. No zero-point corrections have been applied.
[25] C. G. Van de Walle, Phys. Rev. Lett. **80**, 2177 (1998).
[26] J. A. Pople, M. Head-Gordon, D. J. Fox, K. Raghavachary, and L. A. Curtiss, J. Chem. Phys. **90**, 5622 (1989).
[27] A. D. Becke, J. Chem. Phys. **97**, 9173 (1992).
[28] W. B. Fowler, J. K. Rudra, M. E. Zvanut, and F. J. Feigl, Phys. Rev. B **41**, 8313 (1990).
[29] P. Carloni, P. E. Blöchl, and M. Parrinello, J. Phys. Chem. **99**, 1338 (1995).
[30] S. Blügel, H. Akai, R. Zeller, and P. H. Dederichs, Phys. Rev. B **35**, 3271 (1987).
[31] *Quantities, Unities and Symbols in Physical Chemistry*, edited by I. Mills, T. Cvitas, K. Hofmann, N. Kallay, and K. Kuchitsu (Blackwell Scientific Publications, Oxford, 1993).
[32] J. Isoya, J. A. Weil, and L. E. Halliburton, J. Chem. Phys. **74**, 5436 (1981).
[33] W. H. Zachariasen, J. Am. Chem. Soc. **54**, 3842 (1932).
[34] J. Sarnthein, A. Pasquarello, and R. Car, Phys. Rev. Lett. **74**, 4682 (1995).
[35] J. Sarnthein, A. Pasquarello, and R. Car, Phys. Rev. B **52**, 12 690 (1995).
[36] P. E. Blöchl and J. H. Stathis, Physica B **273-274**, 1022 (1999).
[37] A. C. Wright and J. A. E. Desa, Phys. Chem. Glasses **19**, 140 (1978).
[38] S. V. King, Nature (London) **213**, 1112 (1967).
[39] D. R. Hamann, Phys. Rev. B **55**, 14 784 (1997).
[40] C. M. Nelson and R. A. Weeks, J. Am. Ceram. Soc. **43**, 396 (1960).
[41] J. Robertson, J. Phys. C **17**, L221 (1984).
[42] K. C. Snyder and W. B. Fowler, Phys. Rev. B **48**, 13 238 (1993).
[43] D. C. Allan and M. P. Teter, J. Am. Ceram. Soc. **73**, 3247 (1990).
[44] M. Boero, A. Pasquarello, J. Sarnthein, and R. Car, Phys. Rev. Lett. **78**, 887 (1997).
[45] D. L. Griscom and E. J. Friebele, Phys. Rev. B **34**, 7524 (1986).
[46] J. R. Chavez, S. P. Karna, K. Vanheusden, C. P. Brothers, R. D. Pugh, B. K. Singaraju, W. L. Warren, and R. A. B. Devine, IEEE Trans. Nucl. Sci. **44**, 1799 (1997).
[47] G. Pacchioni and G. Ierano, Phys. Rev. Lett. **81**, 377 (1998).
[48] R. A. Weeks, J. Appl. Phys. **27**, 1376 (1956).
[49] R. A. Weeks and C. M. Nelson, J. Am. Ceram. Soc. **43**, 399 (1960).
[50] R. H. Silsbee, J. Appl. Phys. **32**, 1459 (1961).
[51] R. A. Weeks and E. Sonder, in *Paramagnetic Resonance*, edited by W. Low (Academic Press, New York, 1963), Vol. II, p. 869.
[52] M. G. Jani, R. B. Bossoli, and L. E. Halliburton, Phys. Rev. B **27**, 2285 (1983).

[53] W. L. Warren, E. H. Poindexter, M. Offenberg, and W. Müller-Warmuth, J. Electrochem. Soc. **139**, 872 (1992); E. H. Poindexter and W. L. Warren, *ibid.* **142**, 2508 (1995).
[54] F. J. Feigl, W. L. Fowler, and K. L. Yip, Solid State Commun. **14**, 225 (1974).
[55] K. L. Yip and W. B. Fowler, Phys. Rev. B **11**, 2327 (1975).
[56] E. P. O'Reilly and J. Robertson, Phys. Rev. B **27**, 3780 (1983).
[57] J. Robertson, Philos. Mag. B **52**, 371 (1985).
[58] A. H. Edwards and W. B. Fowler, J. Phys. Chem. Solids **46**, 841 (1985).
[59] J. K. Rudra and W. B. Fowler, Phys. Rev. B **35**, 8223 (1987).
[60] G. Pacchioni, A. M. Ferrari, and G. Ierano, Faraday Discuss. **107**, 155 (1997).
[61] B. E. Deal, E. H. Snow, and C. A. Mead, J. Phys. Chem. Solids **27**, 1873 (1966).
[62] A. Yokozawa, A. Oshiyama, Y. Miyamoto, and S. Kumashiro (unpublished).
[63] J. P. Perdew and A. Zunger, Phys. Rev. B **23**, 5048 (1981).
[64] C. Fiori and R. A. B. Devine, Phys. Rev. Lett. Phys. Rev. Lett. **52**, 2081 (1984).
[65] C. L. Marquardt and G. H. Sigel, Jr., IEEE Trans. Nucl. Sci. **NS-22**, 2234 (1975).
[66] K. Vanheusden and A. Stesmans, J. Appl. Phys. **74**, 275 (1993).
[67] C. G. Van de Walle and P. E. Blöchl, Phys. Rev. B **47**, 4244 (1983).
[68] A. Yokozawa and Y. Miyamoto, Phys. Rev. B **55**, 13 783 (1997).
[69] R. E. Stahlbush, E. Cartier, and D. A. Buchanan, Microelectron. Eng. **28**, 15 (1995).
[70] E. Cartier and J. H. Stathis, Microelectron. Eng. **28**, 3 (1995).
[71] F. J. Himpsel, F. R. McFeely, A. Taleb-Ibrahimi, J. A. Yarmoff, and G. Holliger, Phys. Rev. B **38**, 6084 (1988).
[72] J. L. Alay and M. Hirose, J. Appl. Phys. **81**, 1606 (1997).
[73] I refer to Kohn-Sham levels as the one-particle energies of the noninteracting reference system. It is well known that those are not directly related to the levels obtained experimentally.
[74] Z. A. Weinberg and A. Hartstein, J. Appl. Phys. **54**, 2517 (1983).
[75] D. L. Griscom, Phys. Rev. B **40**, 4224 (1989).
[76] R. A. Weeks and M. Abraham, J. Chem. Phys. **42**, 68 (1965).
[77] D. L. Griscom, M. Stapelbroek, and E. J. Friebele, J. Phys. Chem. **78**, 1638 (1983).
[78] J. Neugebauer and C. G. Van de Walle, Phys. Rev. Lett. **75**, 4452 (1995).
[79] H. M. Petrilli, P. E. Blöchl, P. Blaha, and K. Schwarz, Phys. Rev. B **57**, 14 690 (1998).
[80] C. G. Van de Walle, P. J. H. Denteneer, Y. Bar-Yam, and S. T. Pantalides, Phys. Rev. B **39**, 10 791 (1989).
[81] S. Takagi, N. Yasuda, and A. Toriumi (unpublished).
[82] D. J. DiMaria (private communication).
[83] S. Takagi, N. Yasuda, and A. Toriumi, IEEE Trans. Electron Devices **46**, 335 (1999).
[84] S. Takagi, N. Yasuda, and A. Toriumi, IEEE Trans. Electron Devices **46**, 348 (1999).
[85] R. A. Weeks, Phys. Rev. **130**, 570 (1963).
[86] J. K. Rudra, W. B. Fowler, and F. Feigl, Phys. Rev. Lett. **55**, 2614 (1985).
[87] P. M. Lenahan and V. P. Dressendorfer, IEEE Trans. Nucl. Sci. **NS-29**, 1459 (1982).
[88] Y. Roh, L. Trombetta, and J. Stathis, Microelectron. Eng. **22**, 227 (1993).
[89] L. E. Halliburton, B. D. Perlson, R. A. Weeks, J. A. Weil, and M. C. Wintersgill, Solid State Commun. **30**, 575 (1979).
[90] D. L. Griscom and W. B. Fowler, Phys. Rev. B **48**, 13 238 (1993).
[91] S.-H. Lo, D. A. Buchanan, Y. Taur, and W. Wang, IEEE Electron Device Lett. **18**, 209 (1997).
[92] M. Fukuda, W. Mizubayashi, A. Kohno, S. Miyazaki, and M. Hirose, Jpn. J. Appl. Phys., Part 2 **37**, L1534 (1998).
[93] F. J. Feigl and J. H. Anderson, J. Phys. Chem. Solids **31**, 575 (1970).
[94] K. O. Hill and G. Meltz, J. Lightwave Technol. **15**, 1263 (1997).
[95] J. F. Conley and P. M. Lenahan, Appl. Phys. Lett. **62**, 40 (1993).
[96] K. O. Hill, Y. Fuji, D. C. Johnson, and B. S. Kawasaki, Appl. Phys. Lett. **32**, 647 (1978).
[97] P. J. Lemaire, R. M. Atkins, V. Mizrahi, and W. A. Reed, Electron. Lett. **29**, 1191 (1993).
[98] R. B. Devine, D. Mathiot, W. L. Warren, D. M. Fleetwood, and B. Aspar, Appl. Phys. Lett. **63**, 2926 (1993).
[99] The present implementation does not yet include the small augmentation contributions from neighboring sites. This term can be included by evaluating the multipole moments

$$P_{R,l,m}=\int dr(r-R)^l Y^*_{l,m}(r-R)[n^1_s(r)-\tilde{n}^1_s(r)]$$

of the augmentation part of the spin density on all sites. The dipolar interaction resulting from the off-center augmentation densities

$$\Delta W_{i,j}=\sum_{R'\neq R}\left[\partial_i\partial_j-\frac{1}{3}\delta_{i,j}\nabla^2\right]\Bigg|_R\sum_{l,m}\frac{4\pi}{2l+1}Y_{l,m}(r-R')\frac{1}{|r-R'|^{l+1}}P_{R',l,m}$$

is then added to $W_{i,j}$. As a conservative order of magnitude estimate, we consider the proton hyperfine splitting due to an electron located at a distance of 1 Å, which yields 1.4 mT. This must be added to the error bar for nearest-neighbor superhyperfine interactions.